

การศึกษาเชิงทฤษฎีของการแตกตัวเชิงเร่งปฏิกิริยาของ C₅-C₆ แอลเคนเป็น โอลิฟิน

โดยใช้ซีโอไลต์

นางสาวประภาพร กิตติวัฒน์ศักดิ์

จุฬาลงกรณ์มหาวิทยาลัย
CHULALONGKORN UNIVERSITY

บทคัดย่อและแฟ้มข้อมูลฉบับเต็มของวิทยานิพนธ์ตั้งแต่ปีการศึกษา 2554 ที่ให้บริการในคลังปัญญาจุฬาฯ (CUIR)
เป็นแฟ้มข้อมูลของนิสิตเจ้าของวิทยานิพนธ์ ที่ส่งผ่านทางบัณฑิตวิทยาลัย

The abstract and full text of theses from the academic year 2011 in Chulalongkorn University Intellectual Repository (CUIR)
are the thesis authors' files submitted through the University Graduate School.

วิทยานิพนธ์นี้เป็นส่วนหนึ่งของการศึกษาตามหลักสูตรปริญญาวิทยาศาสตรมหาบัณฑิต

สาขาวิชาปิโตรเคมีและวิทยาศาสตร์พอลิเมอร์

คณะวิทยาศาสตร์ จุฬาลงกรณ์มหาวิทยาลัย

ปีการศึกษา 2558

ลิขสิทธิ์ของจุฬาลงกรณ์มหาวิทยาลัย

THEORETICAL STUDY OF CATALYTIC CRACKING OF C₅-C₆ ALKANES
TO OLEFINS USING ZEOLITES

Miss Prapaporn Kittiwattanasak



A Thesis Submitted in Partial Fulfillment of the Requirements
for the Degree of Master of Science Program in Petrochemistry and Polymer Science
Faculty of Science
Chulalongkorn University
Academic Year 2015
Copyright of Chulalongkorn University

Thesis Title THEORETICAL STUDY OF CATALYTIC
CRACKING OF C₅-C₆ ALKANES TO
OLEFINS USING ZEOLITES

By Miss Prapaporn Kittiwattanasak

Field of Study Petrochemistry and Polymer Science

Thesis Advisor Professor Vithaya Ruangpornvisuti, Dr.rer.nat.

Accepted by the Faculty of Science, Chulalongkorn University in Partial
Fulfillment of the Requirements for the Master's Degree

..... Dean of the Faculty of Science
(Associate Professor Polkit Sangvanich, Ph.D.)

THESIS COMMITTEE

..... Chairman
(Associate Professor Vudhichai Parasuk, Ph.D.)

..... Thesis Advisor
(Professor Vithaya Ruangpornvisuti, Dr.rer.nat.)

..... Examiner
(Assistant Professor Prasert Reubroycharoen, Ph.D.)

..... External Examiner
(Assistant Professor Khajadpai Thipayapong, Ph.D.)

CHULALONGKORN UNIVERSITY

ประภาพร กิตติวัฒน์ศักดิ์ : การศึกษาเชิงทฤษฎีของการแตกตัวเชิงเร่งปฏิกิริยาของ C₅–C₆ แอลเคนเป็นโอเลฟินโดยใช้ซีโอไลต์ (THEORETICAL STUDY OF CATALYTIC CRACKING OF C₅–C₆ ALKANES TO OLEFINS USING ZEOLITES) อ.ที่ปริกษาวิทยานิพนธ์หลัก: ศ. ดร.วิทยา เรืองพรวิสุทธิ, 62 หน้า.

กลไกการแตกตัวของ *n*-pentane และ *n*-hexane บนตัวเร่งปฏิกิริยา H-ZSM-5 และ H-FER ถูกศึกษาโดยทฤษฎี ONIOM(B3LYP/6-31+G(d,p):AM1) ด้วยแบบจำลองขนาด 52T และ 64T ตามลำดับ ผลการศึกษาแสดงให้เห็นว่ากระบวนการแตกตัวของ *n*-pentane และ *n*-hexane บนตัวเร่งปฏิกิริยา H-ZSM-5 และ H-FER ประกอบด้วยสองเส้นทางการเกิดปฏิกิริยา เส้นทางการเกิดปฏิกิริยาผันกลับได้ เส้นทางการเกิดตัวขัดขวางตัวเร่งปฏิกิริยา กระบวนการแตกตัวของ *n*-pentane และ *n*-hexane ทั้งที่ใช้ตัวเร่งปฏิกิริยา H-ZSM-5 หรือ H-FER ให้ผลิตภัณฑ์หลักเป็น 1,2-pentene และ 1,2-hexene และให้ 2-pentoxy และ 2-hexoxy เป็นผลิตภัณฑ์ข้างเคียงที่ขัดขวางตัวเร่งปฏิกิริยา ตามลำดับ ปริมาณทางอุณหพลศาสตร์ ค่าคงที่อัตรา ค่าคงที่สมดุล และพลังงานปฏิกิริยาของปฏิกิริยาการแตกตัวของ *n*-pentane และ *n*-hexane บนตัวเร่งปฏิกิริยา H-ZSM-5 และ H-FER ได้ถูกรายงาน

จุฬาลงกรณ์มหาวิทยาลัย
CHULALONGKORN UNIVERSITY

สาขาวิชา ปีโตรเคมีและวิทยาศาสตร์พอลิเมอร์ ลายมือชื่อนิติต

ปีการศึกษา 2558

ลายมือชื่อ อ.ที่ปริกษาหลัก

5572033423 : MAJOR PETROCHEMISTRY AND POLYMER SCIENCE

KEYWORDS: H-ZSM-5 / H-FER / ZEOLITE / N-PENTANE CRACKING / N-HEXANE CRACKING / OLIFINS / ONIOM METHOD

PRAPAPORN KITTIWATTANASAK: THEORETICAL STUDY OF CATALYTIC CRACKING OF C₅-C₆ ALKANES TO OLEFINS USING ZEOLITES. ADVISOR: PROF. VITHAYA RUANGPORNVISUTI, Dr.rer.nat., 62 pp.

The cracking mechanisms of *n*-pentane and *n*-hexane over the H-ZSM-5 and H-FER catalysts were investigated using the ONIOM(B3LYP/6-31+G(d,p):AM1) method with 52T and 64T cluster model, respectively. The computation results show that the cracking process of *n*-pentane and *n*-hexane over the H-ZSM-5 and H-FER catalysts consisting of two reaction paths. The first path is turnover path. The second path is poisoning path. The cracking processes of the *n*-pentane and *n*-hexane over either the H-ZSM-5 or H-FER catalyst afford the 1,2-pentene and 1,2-hexene as the major products and then provide 2-pentoxy and 2-hexoxy species as catalyst poisoning, respectively. Thermodynamic quantities, rate constants, equilibrium constants and reaction energies of cracking reaction of *n*-pentane and *n*-hexane over the H-ZSM-5 and H-FER catalysts are reported.

จุฬาลงกรณ์มหาวิทยาลัย
CHULALONGKORN UNIVERSITY

Field of Study: Petrochemistry and
Polymer Science

Student's Signature

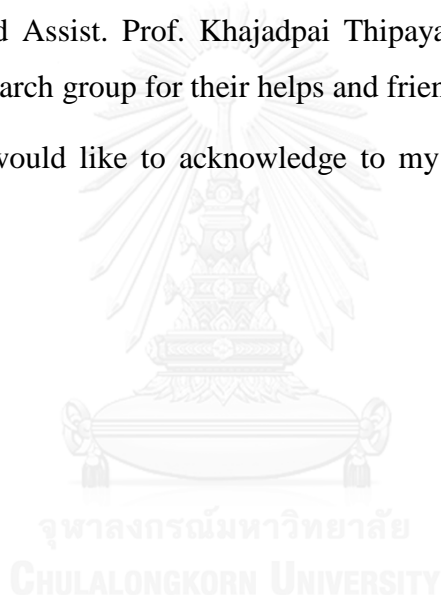
Advisor's Signature

Academic Year: 2015

ACKNOWLEDGEMENTS

The 90th Anniversary of Chulalongkorn University Fund (Ratchadaphiseksomphot Endowment Fund) provided through the Graduate School, Chulalongkorn University, Thailand, granted to Prapaorn Kittiwattanasak is gratefully acknowledged. I would like to express my deep appreciation to my advisor Prof. Dr. Vithaya Ruangpornvisuti who gave me the valuable comments and spent the time helping me to achieve this study. I would also like to thank the committee Assoc. Prof. Dr. Vudhichai Parasuk, Assist. Prof. Prasert Reubroycharoen and Assist. Prof. Khajadpai Thipayapong. I specially thank the members of my research group for their helps and friendship.

Finally, I would like to acknowledge to my family for their supporting and encouragement.



CONTENTS

	Page
THAI ABSTRACT	iv
ENGLISH ABSTRACT.....	v
ACKNOWLEDGEMENTS.....	vi
CONTENTS.....	vii
LIST OF FIGURES	ix
LIST OF TABLES	xiii
LIST OF ABBREVIATIONS AND SYMBOLS	xiv
CHAPTER I INTRODUCTION.....	1
1.1 Background and literature review.....	1
1.2 Zeolite	2
1.2.1 Adsorption of alkanes in zeolite pores	3
1.2.2 Acidity	3
1.3 ZSM-5 zeolite	4
1.4 FER zeolite	5
1.5 Objective.....	6
CHAPTER II THEORY	7
2.1 Semi-empirical method.....	7
2.2 Hartree-Fock method	7
2.3 Density functional theory (DFT)	8
2.3.1 Kohn–Sham orbitals and equations	8
2.3.2 Hybrid functional	10
2.4 Basis sets.....	11
2.4.1 Minimal basis sets	11
2.4.2 Split–valence basis sets	12
2.4.3 Polarized basis sets	12
2.4.4 Diffuse functions	12
2.5 ONIOM method.....	13
2.6 Transition state theory	14

	Page
2.7 Thermochemistry	15
2.7.1 Enthalpies and free energies of reaction.....	15
2.7.2 Rate constant	16
2.7.2.1 Rate constant with tunneling corrections	16
2.7.2.2 Partition functions	17
2.7.2.2.1 Translational partition function	17
2.7.2.2.2 Rotational partition function.....	17
2.7.2.2.3 Vibrational partition function	18
2.7.2.2.4 Electronic partition function	19
CHAPTER III DETAILS OF COMPUTATION	20
3.1 Computational Approach.....	20
3.2 Cluster models for the H-ZSM-5 and H-FER.....	21
3.3 Structure optimization and potential energy surface	23
CHAPTER IV RESULTS AND DISCUSSION	24
4.1 Cracking of <i>n</i> -pentane over the H-ZSM-5	24
4.2 Cracking of <i>n</i> -hexane over the H-ZSM-5	31
4.3 Cracking of <i>n</i> -pentane over the H-FER.....	37
4.4 Cracking of <i>n</i> -hexane over the H-FER.....	43
CHAPTER V CONCLUSION.....	50
REFERENCES	56
APPENDICES	57
VITA	62

LIST OF FIGURES

Figure	Page
1.1 The primary building units of (a) TO_4 tetrahedron (b) TO_4 tetrahedra bridging by a common oxygen.....	2
1.2 Bronsted and Lewis acid sites in zeolites.....	4
1.3 The structure of ZSM-5 zeolite.....	5
1.4 The structure of FER zeolite.....	6
2.1 The ONIOM extrapolation scheme for a molecular system partitioned into two left and three right layers.....	13
2.2 Potential energy profiles of reaction path.....	14
3.1 The cluster models in combination with the two-layer ONIOM approach for (a) the H-ZSM-5 catalyst (denoted by HZ^Z) modeled as the 52T cluster and (b) the H-FER catalyst (denoted by HZ^F) modeled as the 64T cluster. The high and low layers defined in the two-layer ONIOM approach are illustrated as the ball and stick atoms, respectively. The molecular images on the righthand side are the optimized structures for their adsorption configuration with the <i>n</i> -pentane reactant as representatives.....	22
4.1 The cluster models in combination with the two-layer ONIOM approach for (a) the H-ZSM-5 catalyst modeled as the 52T cluster and (b) the H-FER catalyst modeled as the 64T cluster. The H-O bond lengths are in Å. The stretching vibrations are in cm^{-1}	25
4.2 Potential energy profile of the Path C5_Z^Z for <i>n</i> -pentane (C_5) conversion to 1,2-pentene ($\text{C}_5^=$) over the H-ZSM-5 (HZ^Z) catalyst.....	26
4.3 The ONIOM(B3LYP/6-31+G(d,p):AM1)-optimized structures of interaction configurations of the H-ZSM-5 with related species in the cracking process of C_5 reactant to $\text{C}_5^=$ product. For clarity, portions of their molecular structures are depicted. Bond distances are in Å. The single imaginary frequency for transition-state structures is in parentheses.....	2

Figure	Page
4.4 Interatomic distances (in Å) between atoms of the H-ZSM-5 (HZ ^Z) and interacting species for reaction path (Path C5_Z ^Z) of C ₅ conversion to C ₅ ⁼ over the H-ZSM-5 catalyst (Z ^Z H). Atomic symbols with labels are defined in Figure 3.1.....	29
4.5 The ONIOM(B3LYP/6-31+G(d,p):AM1)-optimized structures of (a) the TS3_Z ^Z transition state and (b) 2-pentoxy species on the H-ZSM-5 catalyst. For clarity, portions of the H-ZSM-5 structure are depicted. The single imaginary frequency for transition-state structure is shown in parenthesis.....	31
4.6 Potential energy profile of the Path C6_Z ^Z for <i>n</i> -hexane (C ₆) conversion to 1,2-hexene (C ₆ ⁼) over the H-ZSM-5 (HZ ^Z) catalyst.....	32
4.7 The ONIOM(B3LYP/6-31+G(d,p):AM1)-optimized structures of interaction configurations of the H-ZSM-5 with related species in the cracking process of C ₆ reactant to C ₆ ⁼ product. For clarity, portions of their molecular structures are depicted. Bond distances are in Å. The single imaginary frequency for transition-state structures is in parentheses.....	33
4.8 Interatomic distances (in Å) between atoms of the H-ZSM-5 (HZ ^Z) and interacting species for reaction path (Path C6_Z ^Z) of C ₆ conversion to C ₆ ⁼ over the H-ZSM-5 catalyst (Z ^Z H). Atomic symbols with labels are defined in Figure 3.1.....	35
4.9 The ONIOM(B3LYP/6-31+G(d,p):AM1)-optimized structures of (a) the TS3_Z ^Z transition state and (b) 2-hexoxy species on the H-ZSM-5 catalyst. For clarity, portions of the H-ZSM-5 structure are depicted. The single imaginary frequency for transition-state structure is shown in parenthesis.....	37
4.10 Potential energy profile of the Path C5_Z ^F for <i>n</i> -pentane (C ₅) conversion to 1,2-pentene (C ₅ ⁼) over the H-FER (HZ ^F) catalyst.....	38

Figure	Page
4.11 The ONIOM(B3LYP/6-31+G(d,p):AM1)-optimized structures of interaction configurations of the H-FER with related species in the cracking process of C ₅ reactant to C ₅ ⁼ product. For clarity, portions of their molecular structures are depicted. Bond distances are in Å. The single imaginary frequency for transition-state structures is in parentheses.....	39
4.12 Interatomic distances (in Å) between atoms of the H-FER (HZ ^F) and interacting species for reaction path (Path C5_Z ^F) of C ₅ conversion to C ₅ ⁼ over the H-FER catalyst (Z ^F H). Atomic symbols with labels are defined in Figure 3.1.....	41
4.13 The ONIOM(B3LYP/6-31+G(d,p):AM1)-optimized structures of (a) the TS3_ZF transition state and (b) 2-pentoxy species on the H-FER catalyst. For clarity, portions of the H-FER structure are depicted. The single imaginary frequency for transition-state structure is shown in parenthesis.....	43
4.14 Potential energy profile of the Path C6_Z ^F for <i>n</i> -hexane (C ₆) conversion to 1,2-hexene (C ₆ ⁼) over the H-FER (HZ ^F) catalyst.....	44
4.15 The ONIOM(B3LYP/6-31+G(d,p):AM1)-optimized structures of interaction configurations of the H-FER with related species in the cracking process of C ₆ reactant to C ₆ ⁼ product. For clarity, portions of their molecular structures are depicted. Bond distances are in Å. The single imaginary frequency for transition-state structures is in parentheses.....	45
4.16 Interatomic distances (in Å) between atoms of the H-FER (HZ ^F) and interacting species for reaction path (Path C6_Z ^F) of C ₆ conversion to C ₆ ⁼ over the H-FER catalyst (Z ^F H). Atomic symbols with labels are defined in Figure 3.1.....	47

Figure	Page
4.17 The ONIOM(B3LYP/6-31+G(d,p):AM1)-optimized structures of (a) the TS3_Z ^F transition state and (b) 2-hexoxy species on the H-FER catalyst. For clarity, portions of the H-FER structure are depicted. The single imaginary frequency for transition-state structure is shown in parenthesis.....	49



LIST OF TABLES

Table	Page
4.1	Reaction energies, thermodynamic properties, rate and equilibrium constants in the <i>n</i> -pentane cracking over the H-ZSM-5 catalyst..... 30
4.2	Reaction energies, thermodynamic properties, rate and equilibrium constants in the <i>n</i> -hexane cracking over the H-ZSM-5 catalyst..... 36
4.3	Reaction energies, thermodynamic properties, rate and equilibrium constants in the <i>n</i> -pentane cracking over the H-FER catalyst..... 42
4.4	Reaction energies, thermodynamic properties, rate and equilibrium constants in the <i>n</i> -hexane cracking over the H-FER catalyst..... 48
A-1	Optimized geometrical distances (in Å) between atoms of H-ZSM-5 and interacting species for reaction path of <i>n</i> -pentane (C ₅) conversion to 1,2-pentene (C ₅ [≡]) over the H-ZSM-5 catalyst..... 58
A-2	Optimized geometrical distances (in Å) between atoms of H-ZSM-5 and interacting species for reaction path of <i>n</i> -hexane (C ₆) conversion to 1,2-hexene (C ₆ [≡]) over the H-ZSM-5 catalyst..... 58
A-3	Optimized geometrical distances (in Å) between atoms of H-FER and interacting species for reaction path of <i>n</i> -pentane (C ₅) conversion to 1,2-pentene (C ₅ [≡]) over the H-FER catalyst..... 59
A-4	Optimized geometrical distances (in Å) between atoms of H-FER and interacting species for reaction path of <i>n</i> -hexane (C ₆) conversion to 1,2-hexene (C ₆ [≡]) over the H-FER catalyst..... 59
A-5	Partition function, Tunneling coefficients (κ) and A factor in the <i>n</i> -pentane cracking over the H-ZSM-5 catalyst..... 60
A-6	Partition function, Tunneling coefficients (κ) and A factor in the <i>n</i> -hexane cracking over the H-ZSM-5 catalyst..... 60
A-7	Partition function, Tunneling coefficients (κ) and A factor in the <i>n</i> -pentane cracking over the H-FER catalyst..... 61
A-8	Partition function, Tunneling coefficients (κ) and A factor in the <i>n</i> -hexane cracking over the H-FER catalyst..... 61

LIST OF ABBREVTATIONS AND SYMBOLS

\AA	Angstrom
B3LYP	Becke 3-Paramater, Lee, Yang and Parr
DFT	Density functional theory
E	Energy
FER	Ferrierite
G	Gibbs free energy
H	Enthalpy
HF	Hartree-Fock
h	Plank's constant
k	Rate constant
k_B	Boltzman's constant
K	Equilibrium constant
Q	Partition function
R	Gas constant
S	Entropy
T	Absolute temperature
TS	Transition state
ZPVE	Zero point vibrational energy
ψ	Wave function
κ	Kappa
ν_i	Imaginary frequency
ZSM-5	Zeolite Socony Mobil Number 5

CHAPTER I

INTRODUCTION

1.1 Background and literature review

Light olefins such as ethene, propene and butenes were obtained from the cracking of *n*-heptane using various zeolites as catalysts [1]. In a fluid catalytic cracking process, ZSM-5 (Zeolite Socony Mobil-5) is widely used as size of additive for light olefin production and gasoline improvement [2]. Uniform H-ZSM-5 was found to show a selective formation and high deactivation resistance of propene and light olefin [3].

There are many works on catalytic cracking of olefins with different number of carbons on zeolite catalysts [4-7]. The catalytic cracking of 2-methyl-2-butene and 2-pentene to form ethylene and propylene over proton-exchanged zeolites [4] and 1-butene to propene over the ZSM-5 catalyst [5] were inspected. The initial reactions of catalytic cracking of 1-butene to produce propene and ethene on zeolites H-ZSM-5 and H-FAU (Faujasite) were theoretically investigated using the ONIOM(B3LYP/6-31G(d,p):B3LYP/3-21G) method [6]. The cracking mechanism of 1-hexane over the H-ZSM-5 zeolite was investigated using the ONIOM(B3LYP/6-31G(d,p):UFF) method [7].

The possibilities of catalytic cracking of naphtha on zeolites IM-5 [8], ZSM-5 [9], MOR (Mordenite) [10] and FER (Ferrierite) [11] were explored. The chemical mechanisms of catalytic cracking of alkanes and alkenes over solid acidic catalysts as well as zeolites were reviewed [12]. The alkane crackings on zeolites MFI and FAU [13] and zeolite H-ZSM-5 [14] were theoretically studied using DFT (density functional theory) methods. The rate constants for reactions and activation energies of *n*-hexane cracking over ZSM-5 zeolites with various Si/Al ratios and crystal sizes [15] and the characterization of the used catalysts were studied [16]. The effect of the crystal size of ZSM-5 zeolite on the catalytic activity and light olefins yield in the catalytic cracking of *n*-hexane were investigated [17]. The effects of steaming on the acidity and catalytic performance of H-ZSM-5 and P/H-ZSM-5 with various Si/Al ratios in the catalytic cracking of heptane were studied [18].

1.2 Zeolite

Three-dimensional four-connected framework in zeolite was constructed from TO_4 tetrahedra which T refers to Si and Al atoms. TO_4 tetrahedra are called primary building units which is the basic structural building units of a zeolite framework as shown in Figure 1.1.

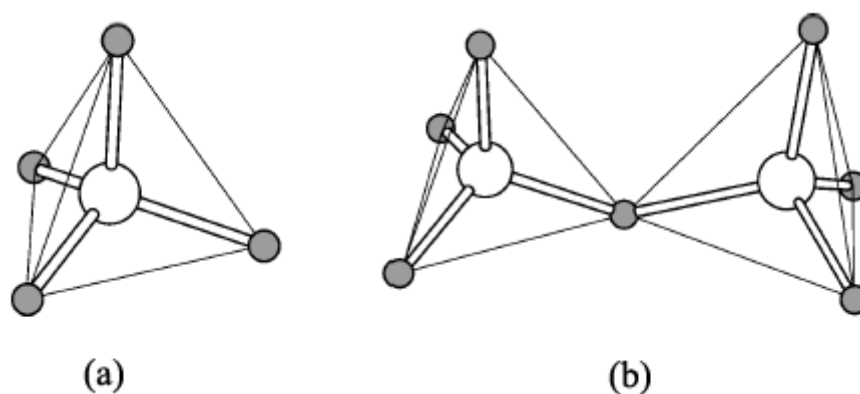


Figure 1.1 The primary building units of (a) TO_4 tetrahedron (b) TO_4 tetrahedra bridging by a common oxygen [19].

Such aluminosilicate are amorphous and much interest has been shown in recent years in crystalline aluminosilicates having the general formula can be written as, $\text{M}_v(\text{AlO}_2)_x(\text{SiO}_2)_y \cdot z\text{H}_2\text{O}$, where M is monovalent cation (e.g. sodium or ammonium), v equals x ; for divalent cations, v is $x/2$ and z is number of water molecule contained in the channels of zeolite. In the channels, there are the cations and adsorbed water molecules.

1.2.1 Adsorption of alkanes in zeolite pores

Zeolite is excellent microporous adsorbent for small medium sizes of gases and liquids because of its pore size and very large surface areas. Chain length and pore dimension are main parameters for normal alkanes adsorption in zeolite pores. The interaction is mainly controlled by dispersive force, which is the van der Waals interaction. In proton-exchanged zeolites case, a smaller contribution is a dipole–dipole-induced interaction with the Brønsted acid site. In zeolite pores, other cations also interact with adsorbate. The longer alkanes can adsorb with the higher heat of adsorption because they are mainly controlled by the van der Waals interaction. In the repeated reporting, heat of adsorption linearly increases when chain length increase [20, 21]. Alkanes are perfectly absorbed in middle pore sizes when the heat is higher in the adsorption proceeding [22].

1.2.2 Acidity

Charge of zeolite comprising Si-O tetrahedral called as silicalite is neutral. The unbalance of the metal and the oxygen charge in the primary building unit. Replacing one Si^{4+} atom in silicalites by Al^{3+} a formal negative charge. This negative charge is then balanced by a proton or metal cation. The framework morphology, type of cation has an influence the acid properties of zeolites as well. From a structural point of view, the bridging hydroxyl groups, which are protons associated with negatively charged framework oxygen's linked into alumina tetrahedra, are the Brønsted acid sites as shown in Figure 1.2. These protons are lost at high temperatures as water molecules followed by the formation of Lewis acid sites as shown in Figure 1.2 [23].

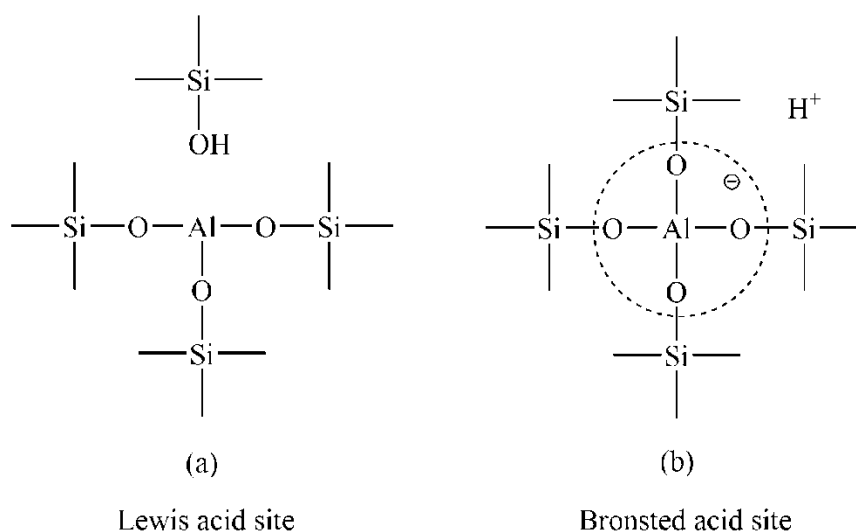


Figure 1.2 Brønsted and Lewis acid sites in zeolites.

1.3 ZSM-5 zeolite

ZSM-5, a highly porous material, it has an intersecting two-dimensional pore structure. There are two types of ZSM-5 pores which both are constructed by 10-membered oxygen rings. The first type is straight and elliptical in cross section. The second type, pore intersects the straight pores at right angles, in a zig-zag pattern and circulating in cross section. They were able to be explained by a shorthand notation of $[100] 5.1 \times 5.5 \text{ \AA}$ and $[010] 5.4 \times 5.6 \text{ \AA}$ as displayed in Figure 1.3. The unit cell of MFI structure is orthorhombic ($a = 20.1$, $b = 19.7$, $c = 13.1 \text{ \AA}$) with Pnma symmetry. The all-silica analogue of zeolite ZSM-5, silicalite-1 is also able to form. Balancing the negative charge of the framework with the additional presence of positive charge is required by the substitution of an aluminum ion for a silicon ion. The additional proton is the reason of causing a high level of acidity in zeolite (H-ZSM-5). The acidic catalytical activity of H-ZSM-5 is affected by the Al component in the framework. One of the most important molecular sieves catalysis materials in the petroleum industry is ZSM-5-type [19].

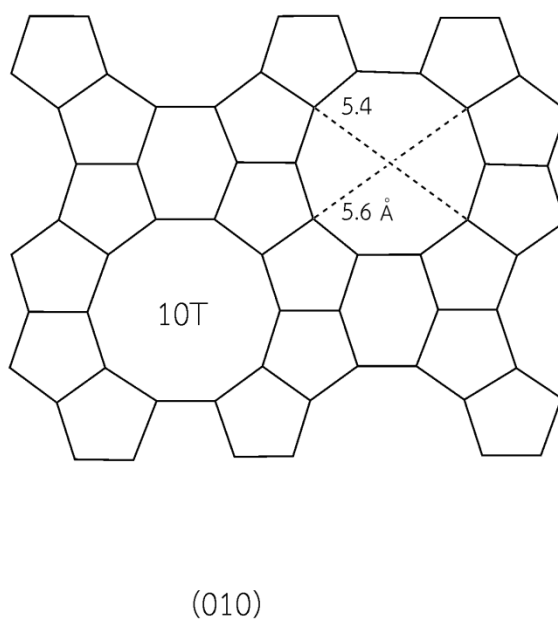


Figure 1.3 The structure of ZSM-5 zeolite. Lengths of pore channel are in Å. Pore size is in unit of T (tetrahedral) [24].

1.4 FER zeolite

The two dimensional pore structure of FER is shown in Figure 1.4. It comprises straight 10-ring channels parallel to the z-axis which is interconnected by cages with 8-ring windows in the y-direction. The pore diameter size of 10-ring channels is [001] 5.4×4.2 Å. FER structure has the space group Immm and the orthorhombic symmetry crystal with $a = 19.02$, $b = 14.30$ and $c = 7.54$ Å) with unit cell dimension [25].

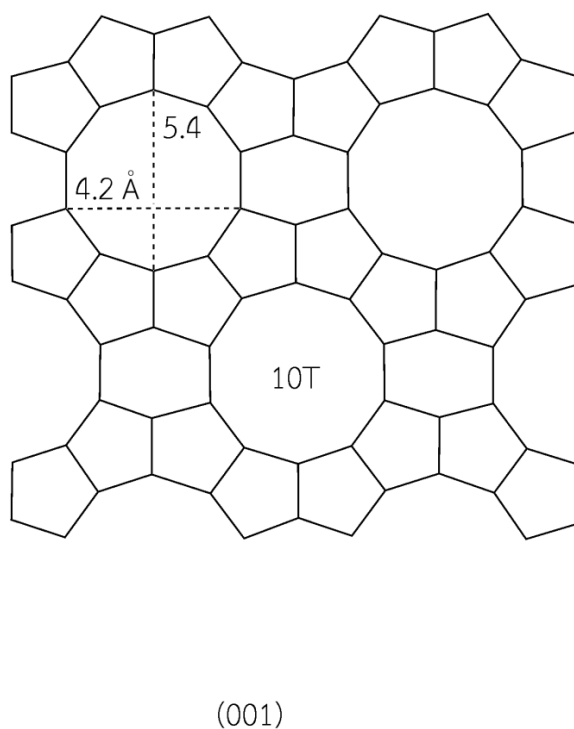


Figure 1.4 The structure of FER zeolite. Lengths of pore channel are in Å. Pore size is in unit of T (tetrahedral) [24].

1.5 Objective

In this study, to rationalize on the experiments of the cracking reactions of *n*-pentane and *n*-hexane over the H-ZSM-5 and H-FER catalysts, a theoretical investigation of reaction mechanisms of the cracking of *n*-pentane and *n*-hexane over the H-ZSM-5 and H-FER catalysts for productions of 1,2-pentene and 1,2-hexene, respectively. The reaction energies, thermodynamic quantities, rate and equilibrium constants of the cracking of the *n*-pentane and *n*-hexane over the H-ZSM-5 and H-FER catalysts have been obtained using the ONIOM(B3LYP/6-31+G(d,p):AM1) method in combination with 52T and 64T cluster models of zeolites, respectively.

CHAPTER II

THEORY

The electronic wave function of polyatomic molecule depends on several parameters—the bond distances, bond angles, and dihedral angles of rotation about single bonds. A full theoretical treatment of a polyatomic molecule involves calculation of the electronic wave function for a range of each of these parameters. The equilibrium bond distances and angles are then found as those values that minimize the electronic energy including nuclear repulsion. The four main approaches for calculations of electronic properties of molecules, are ab initio, semiempirical and the density-functional methods [26].

2.1 Semi-empirical method

Due to limitations of computation to treat molecular systems with large numbers of electrons, ab initio methods are not applied routinely to molecules with several atoms. Semiempirical methods are therefore applied to larger systems and make electronic structure calculations available. Base on experimental data, parameters of atoms optimized to reproduce a number of important chemical properties are included in semiempirical methods. In 1985, Dewar developed an improved version of MNDO called AM1 (Austin model 1) which overcomes the major weaknesses of MNDO without any significant increase in computing time. AM1 provides more accurate enthalpies of formation and ionization energies than MNDO [27].

2.2 Hartree-Fock method

The ab initio methods start with the Hartree–Fock (HF) approximation in that the HF equations which are first solved to find spinorbitals that can then be used to construct configuration state functions. Nevertheless, they do have limitations, in particular the computational difficulty of performing accurate calculations with large basis sets on molecules containing many atoms and many electrons [27].

The molecular HF wave function is written as an antisymmetrized product called Slater determinant of spin-orbitals, each spin-orbital being a product of a spatial orbital and spin function. The HF molecular electronic energy E_{HF} is given by the variation theorem. Therefore, the HF energy of a diatomic or polyatomic molecule with closed shells is expressed as Equation (2.1) [26].

$$E_{HF} = 2 \sum_{i=1}^{n/2} H_{ii}^{core} + \sum_{i=1}^{n/2} \sum_{j=1}^{n/2} (2J_{ij} - K_{ij} + V_{NN}) \quad (2.1)$$

where H_{ii}^{core} is one-electron-operator symbol, J_{ij} is coulomb integrals, K_{ij} is exchange integrals, $n/2$ is occupied spatial orbitals of n -electron molecule and V_{NN} is nuclear repulsion energy.

2.3 Density functional theory (DFT)

An alternative to the HF methods that is also popular among quantum chemists is density functional theory (DFT). The basic idea behind DFT is that the energy of an electronic system can be written in terms of the electron probability density, ρ . For a system of n electrons, $\rho(r)$ denotes the total electron density at a particular point r in space. The electronic energy E is said to be a functional of the electron density and is denoted $E[\rho]$, in the sense that for a given function $\rho(r)$, there is a single corresponding energy.

2.3.1 Kohn–Sham orbitals and equations

The concept of a density functional for the energy was the basis of some early but useful approximate models such as the Thomas–Fermi method and the Hartree–Fock–Slater or $X\alpha$ method. Nevertheless, formal proof was given by P. Hohenberg and W. Kohn that the ground-state energy and all other ground-state electronic properties are uniquely determined by the electron density. In the development of DFT came with the derivation of a set of one-electron equations from which the electron density could be obtained. Systems in which paired electrons are described

by the same spatial one-electron orbitals as in restricted Hartree–Fock theory were therefore considered. W. Kohn and L.J. Sham showed that the exact ground-state electronic energy E of an n -electron system can be written as Equation (2.2).

$$E[\rho] = -\frac{\hbar^2}{2m_e} \sum_{i=1}^n \int \psi_i^*(r_1) \nabla_1^2 \psi_i(r_1) dr_1 - j_0 \sum_{I=1}^N \frac{Z_I}{r_{I1}} \rho(r_1) dr_1 + \frac{1}{2} j_0 \int \frac{\rho(r_1)\rho(r_2)}{r_{12}} dr_1 dr_2 + E_{XC}[\rho] \quad (2.2)$$

where the one-electron spatial orbitals ψ_i ($i=1, 2, \dots, n$) are the Kohn–Sham orbitals, the solutions of the equations given below. The exact ground-state electron density is given as Equation (2.3).

$$\rho(r) = \sum_{i=1}^n |\psi_i(r)|^2 \quad (2.3)$$

where the sum is over all the occupied Kohn–Sham (KS) orbitals; ρ is known once these orbitals have been computed.

The first term on the right in Equation (2.2) represents the kinetic energy of the electrons. The second term represents the electron–nucleus attraction where the sum is over all N nuclei with index I and atomic number Z_I . The third term represents the Coulomb interaction between the total charge distribution at r_1 and r_2 . The last term is the exchange–correlation energy of the system, which is also a functional of the density and takes into account all non-classical electron–electron interactions. Among the four terms, E_{XC} is the one which does not obtain exactly. Although the Hohenberg–Kohn theorem tells that E and E_{XC} must be functionals of the electron density. The KS orbitals are found by solving the Kohn–Sham equations, which are derived by applying the variation principle to the electronic energy $E[\rho]$ with the charge density given by Equation (2.3). The KS equations for the one electron orbitals $\psi_i(r_1)$ are in a form as Equation (2.4).

$$\left\{ -\frac{\hbar^2}{2m_e} \nabla_1^2 - j_0 \sum_{I=1}^N \frac{Z_I}{r_{I1}} + j_0 \int \frac{\rho(r_2)}{r_{12}} dr_2 + V_{XC}(r_1) \right\} \psi_i(r_1) = \varepsilon_i \psi_i(r_1) \quad (2.4)$$

where ε_i are the KS orbital energies and the exchange–correlation potential, V_{xc} , is the functional derivative of the exchange–correlation energy as shown in Equation (2.5) [27].

$$V_{xc}[\rho] = \frac{\delta E_{xc}[\rho]}{\delta \rho} \quad (2.5)$$

2.3.2 Hybrid functional

The most popular hybrid functional at present is based on an exchange-energy functional developed by Becke in 1993, and modified by Stevens et al. in 1994 by introduction of LYP 1988 correlation-energy functional. This exchange–correlation functional, called the Becke3LYP or B3LYP functional is expressed as Equation (2.6).

$$E_{xc}^{B3LYP} = (1 - a_0 - a_x)E_x^{LSDA} + a_0E_x^{HF} + a_xE_x^{B88} + (1 - a_c)E_c^{VWN} + a_cE_c^{LYP} \quad (2.6)$$

where E_x^{LSDA} is the kind of accurate LSDA non-gradient-corrected exchange functional, E_x^{HF} is the KS-orbital-based HF exchange energy functional, E_x^{B88} is the Beck 88 exchange functional mentioned above, E_c^{VWN} is the Vosko, Wilk, Nusair function (SVWN function), which forms part of the accurate functional for the homogeneous electron gas of LDA and the LSDA, and E_c^{LYP} is the LYP correlation functional mentioned above. E_x and E_c of the last three terms are gradient-corrected. The parameters a_0 , a_x and a_c are obtained from the best fit of the calculated energy to molecular atomization energies [28].

2.4 Basis sets

The Slater-type orbitals (STOs) is written as Equation (2.7).

$$\psi_{nlm_l}(r, \theta, \phi) = Nr^{n_{eff}-1} e^{-Z_{eff}r} Y_{lm_l}(\theta, \phi) \quad (2.7)$$

where n , l , and m_l are quantum numbers, Z is atomic number, N is a normalization constant, Y_{lm_l} is a spherical harmonic, $\rho = r/a_0$, n_{eff} is effective principal quantum number and Z_{eff} is effective nuclear charge.

A complete basis set consists of STOs with all permitted integral values of n , l , and m_l and all positive values of the orbital exponents, ζ (zeta), the parameter that occurs in the radial part ($e^{-\zeta r}$) of the STO. In practice, only a small number of all possible functions are used. The best values of ζ are determined by fitting STOs to the numerically computed atomic wavefunctions. For atomic self-consistent field (SCF) calculations, STO basis functions are centred on the atomic nucleus. For diatomic and polyatomic species, STOs are centred on each of the atoms. However, for HF-SCF calculations on molecules with three or more atoms, the evaluation of the many two-electron integrals ($ab|cd$) is impractical. Indeed, this ‘two-electron integral problem’ was once considered to be one of the greatest problems in quantum chemistry [27].

2.4.1 Minimal basis sets

The simplest type of basis set is a minimal basis set in which one function is used to represent each of the orbitals of elementary valence theory. A minimal basis set would include one function each for H and He for the 1s-orbital, five basis functions each for Li to Ne for the 1s-, 2s-, and three 2p-orbitals, and nine functions each for Na to Ar, and so on. However, a minimal basis set results in wavefunctions and energies that are not very close to the Hartree–Fock limits: accurate calculations need more extensive basis sets [27].

2.4.2 Split-valence basis sets

A split-valence (SV) basis set is a compromise between the inadequacy of a minimal basis set and the computational demands of double-zeta (DZ) and triple-zeta (TZ) basis sets. Each valence atomic orbital is represented by two basis functions while each inner-shell atomic orbital is represented by a single basis function. In 3-21G basis set, one contracted Gaussian composed of three primitives is used to represent each inner-shell atomic orbital. Each valence-shell orbital is represented by two functions, one a contracted Gaussian of two primitives and one a single (and usually diffuse) primitive. The primitives are first optimized in an SCF calculation on atoms, and the contracted sets are then used in molecular calculations [27].

2.4.3 Polarized basis sets

The 6-31G* basis set starts with the split-valence 6-31G basis and adds polarization functions in the form of six d-type functions for each atom other than H. Another star, an additional polarization function: 6-31G** indicates the addition to 6-31G of a set of three p-type polarization functions for each H atom [27].

2.4.4 Diffuse functions

Anions, compound with lone pairs, and hydrogen-bonded dimer have significant electron density at large distance from the nuclei. To improve the accuracy for such compounds, the 3-21+G and 6-31+G* basis sets formed from the 3-21G and 6-31G* sets by the addition of four highly diffuse functions (s , p_x , p_y , p_z) on each non-hydrogen atom; a highly diffuse function is one with a very small orbital exponent. The 3-21++G and 6-31++G* sets also include a highly diffuse s function on each hydrogen atom [26].

2.5 ONIOM method

ONIOM stands for our own N-layered Integrated molecular Orbital. The basic idea behind ONIOM approach can be explained most easily when it is considered as an extrapolation scheme in a two-dimensional space, spanned by the size of the system on one axis and the level of theory on the other axis. The extrapolation procedure schematically shown in Figure 2.1 describes the real system at the highest level of theory, i.e. the approximation of the target E_4 (point 4) in a system partitioned into the two-layer ONIOM or E_9 (point 9) in a system consisting of three layers.

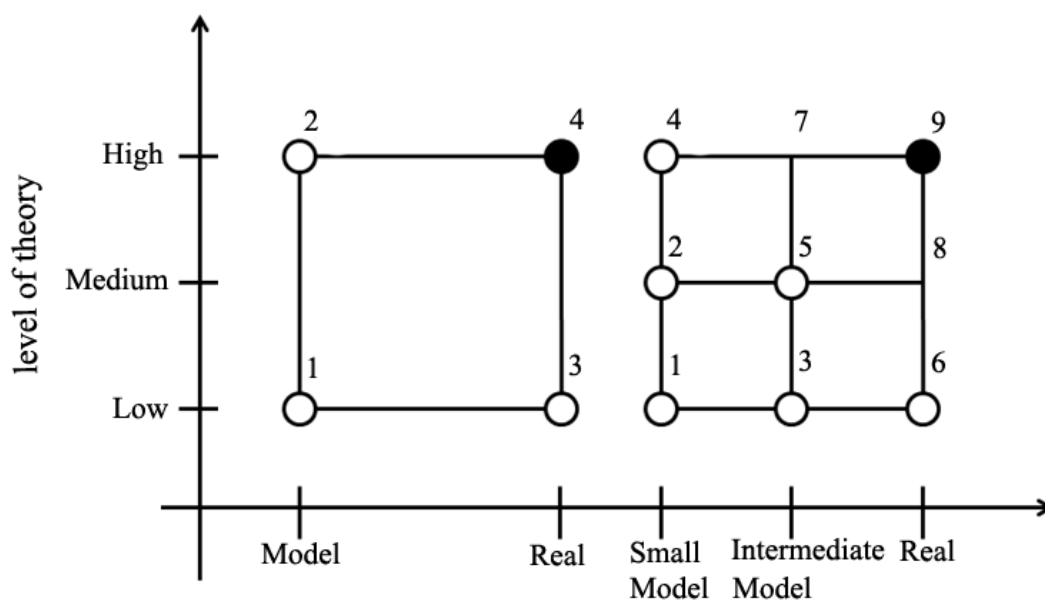


Figure 2.1 The ONIOM extrapolation scheme for a molecular system partitioned into two left and three right layers.

In the case of two layers, the extrapolated energy E_{ONIOM2} is then defined as Equation (2.8).

$$E_{\text{ONIOM2}} = E_3 - E_1 + E_2 \quad (2.8)$$

where E_3 is the energy of the entire system or real system which is calculated at the low level of theory. E_1 and E_2 are the energies of the model system determined at the low and high level of theory, respectively. E_{ONIOM2} is an approximation to the true energy of the real system E_4 which is obtained using Equation (2.9).

$$E_4 = E_{\text{ONIOM2}} + D \quad (2.9)$$

where D is error of the extrapolation [29].

2.6 Transition state theory

Transition state theory (TST) provides an approach to explain the temperature and concentration dependence of the rate law. On this potential energy surface there will be a path of minimum energy expenditure for the reaction to proceed from reactants to products (reaction coordinate). The low energy positions of reactants and products on the potential energy surface will be separated by a higher energy region. The highest energy along the minimum energy pathway in going from reactants to products defines in chemistry; TST is a conception of chemical reactions involving rearrangement of species as transition state (TS). TS is the configuration which divides the reactant and product parts of surface as shown in Figure 2.2 [30].

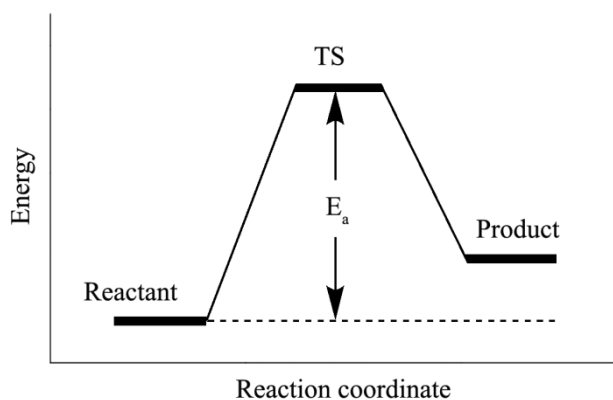


Figure 2.2 Potential energy profile of reaction path.

2.7 Thermochemistry

2.7.1 Enthalpies and free energies of reaction

The difference of the sums of heat formation is taken to calculate the enthalpies of reaction using Equation (2.10).

$$\Delta_r H^\circ(298K) = \sum_{prod} \Delta_f H^\circ_{prod}(298K) - \sum_{react} \Delta_f H^\circ_{react}(298K) \quad (2.10)$$

The enthalpy of reaction can be calculated by Equation (2.11).

$$\Delta_r H^\circ(298K) = \sum_{prod} (\varepsilon_0 + H_{corr}) - \sum_{react} (\varepsilon_0 + H_{corr}) \quad (2.11)$$

where H° is standard enthalpy. ε_0 is the total electronic energy. H_{corr} is correction enthalpies due to internal energy which can be calculated by Equation (2.12).

$$H_{corr} = E_{tot} + k_B T \quad (2.12)$$

where k_B is Boltzmann constant (1.380662×10^{-23} J/K). T is temperature (default is 298.15). E_{tot} , total internal energy, is the sum of E_t , E_r , E_v , E_e which are internal energy due to transition, rotational, vibrational and electronic motion, respectively, as shown in Equation (2.13).

$$E_{tot} = E_t + E_r + E_v + E_e \quad (2.13)$$

The Gibbs free energies of reaction can be calculated using Equation (2.14).

$$\Delta_r G^\circ(298K) = \sum_{prod} (\varepsilon_0 + G_{corr}) - \sum_{react} (\varepsilon_0 + G_{corr}) \quad (2.14)$$

where G° is standard Gibbs free energy. The correction to Gibbs free energy due to internal energy (G_{corr}) can be calculated using Equation (2.15).

$$G_{corr} = H_{corr} - TS_{tot} \quad (2.15)$$

where S_{tot} is total internal entropy which is the sum of internal energy due to transition (S_t), rotational (S_r), vibrational (S_v) and electronic motion (S_e) [31].

2.7.2 Rate constant

2.7.2.1 Rate constant with tunneling corrections

The Gibbs free energy change ΔG_{298}^o and standard enthalpy ΔH_{298}^o of all studied reactions have been derived from the zero-point vibrational energy (ZPVE) [32] under the ONIOM(B3LYP/6-31+G(d,p):AM1) method. The rate constants $k(T)$ of each reaction step via its corresponding transition state derived from the transition-state theory were computed from activation energy (ΔE^\ddagger) using Equation (2.16) [32, 33].

$$k(T) = \kappa \frac{k_B T}{h} \frac{Q_{TS}}{Q_{REA}} e^{-\frac{\Delta E^\ddagger}{RT}} \quad (2.16)$$

where κ is tunneling coefficient, k_B is the Boltzmann's constant, h is Plank's constant, T is the absolute temperature at 298.15 K, R is the gas constant value of 1.987×10^{-3} kcal mol⁻¹T⁻¹, and Q_{TS} and Q_{REA} are the partition function of translational, rotational, and vibrational partition functions from the zero-point vibrational energy (ZPVE).

The tunneling coefficient can be computed with the Wigner method [34, 35] as $\kappa = 1 + (1/24)(h\nu_i/c/k_B T)^2$, where c is speed of light and ν_i is the imaginary frequency that accounts for the vibration motion along the reaction path. The pre-exponential factor (A) is defined in Equation (2.17).

$$A = \frac{k_B T}{h} \frac{Q_{TS}}{Q_{REA}} \quad (2.17)$$

The equilibrium constant (K) is defined using a thermodynamic Equation (2.18) at 298.15 K and 1 atm.

$$K = e^{-\frac{\Delta G}{RT}} \quad (2.18)$$

2.7.2.2 Partition functions

The total partition function (Q) can be approximated as a product of translational, rotational, vibrational, and electronic partition functions as shown in Equation (2.19) [31].

$$Q = Q_t Q_r Q_v Q_e \quad (2.19)$$

where Q_e is electronic partition function, Q_r is rotational partition function, Q_t is translational partition function and Q_v is vibrational partition function.

2.7.2.2.1 Translational partition function

The translational partition function is written as shown in Equation (2.20).

$$Q_t = \left(\frac{2\pi m k_B T}{h^2} \right)^{3/2} V \quad (2.20)$$

where m is the mass of the molecule and V is the molar volume at specific volume and pressure in a gas phase system [31].

2.7.2.2.2 Rotational partition function

The discussion for molecular rotation can be divided into several cases: single atoms, linear polyatomic molecules, and general non-linear polyatomic molecules. For a linear molecule, the rotational partition function is written as shown in Equation (2.21).

$$Q_r = \frac{1}{\sigma_r} \left(\frac{T}{\Theta_r} \right) \quad (2.21)$$

where $\Theta_r = h^2 / 8\pi^2 I k_B$. $\Theta_{r(x,y,z)}$ is characteristic temperature for rotation (in the x, y or z plane). I is the moment of inertia.

For the general case for a nonlinear polyatomic molecule, the rotational partition function is written as shown in Equation (2.22). [31]

$$Q_r = \frac{\pi^{1/2}}{\sigma_r} \left(\frac{T^{3/2}}{(\Theta_{r,x} \Theta_{r,y} \Theta_{r,z})^{1/2}} \right) \quad (2.22)$$

2.7.2.2.3 Vibrational partition function

The contributions to the partition function, entropy, internal energy and constant volume heat capacity from vibrational motions are composed of a sum (or product) of the contributions from each vibrational mode, K. The first vibrational energy level to be the zero of energy ($V=0$), then the partition function for each vibrational level is written as shown in Equation (2.23).

$$Q_{v,K} = \frac{1}{1 - e^{-\Theta_{v,K}/T}} \quad (2.23)$$

where $\Theta_{v,K} = hv_K / k_B$ is characteristic temperature for vibration K.

The overall vibrational partition function is written as shown in Equation (2.24) [31].

$$Q_v = \prod_K \frac{1}{1 - e^{-\Theta_{v,K}/T}} \quad (2.24)$$

2.7.2.2.4 Electronic partition function

The electronic partition function is shown in Equation (2.25).

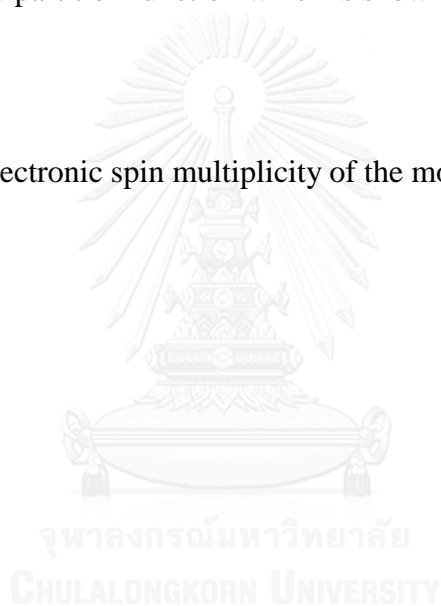
$$Q_e = \omega_0 e^{-\epsilon_0/k_B T} + \omega_1 e^{-\epsilon_1/k_B T} + \omega_2 e^{-\epsilon_2/k_B T} + \dots \quad (2.25)$$

where ω_n is the degeneracy of the n-th energy level, ϵ_n is the energy of the n-th level.

The first electronic excitation energy is assumed to be much greater than $k_B T$. Therefore, the first and higher excited states are assumed to be inaccessible at any temperature. Thus, the energy of the ground state is set to zero. These assumptions simplify the electronic partition function which is shown in Equation (2.26).

$$Q_e = \omega_0 \quad (2.26)$$

which is the simply electronic spin multiplicity of the molecule [31].



CHAPTER III

DETAILS OF COMPUTATION

3.1 Computational Approach

The two-layer ONIOM approach [36, 37] employed together with cluster models for the H-ZSM-5 and H-FER catalysts have been modeled by the 52T ($\text{H}_{40}\text{Si}_{51}(\text{HO})\text{AlO}_{83}$) and 64T ($\text{H}_{52}\text{Si}_{63}(\text{HO})\text{AlO}_{101}$) clusters, respectively. The high zones of zeolite molecules describing in the two-layer ONIOM method assigned for the H-ZSM- and H-FER cluster models are shown as ball atoms which are the 22T ($\text{H}_{10}\text{Si}_{21}(\text{HO})\text{AlO}_{46}$) and 20T ($\text{Si}_{19}(\text{HO})\text{AlO}_{23}$) components, respectively, see Figure 3.1. The two-layer ONIOM approach, high and low regions are treated using the B3LYP/6-31+G(d,p) [38-40] and the AM1 [41] methods as high and low levels of theory, respectively. For clear definition, the ONIOM(B3LYP/6-31+G(d,p):AM1)-optimized structures of the H-ZSM-5, H-FER clusters and their *n*-pentane adsorption configurations are shown in Figure 3.1.

The structure optimizations of the H-ZSM-5 (52T), H-FER (64T) clusters, their interaction configurations with *n*-pentane, *n*-hexane reactants, related intermediates, 1,2-pentene, 1,2-hexene products and their corresponding transition states have been carried out using the ONIOM(B3LYP/6-31+G(d,p):AM1) method. All calculations were performed using the GAUSSIAN 09 program [42] and their structures were visualized using the MOLEKEL 4.3 program [43]. The zero-point energies (ZPE) and thermodynamic properties based on the vibrational energy (ZPVE) corrections derived from frequency calculations at the ONIOM(B3LYP/6-31+G(d,p):AM1) level were achieved.

3.2 Cluster models for the H-ZSM-5 and H-FER

The initial structures of H-ZSM-5 modeled as 52T ($H_{40}Si_{51}(HO)AlO_{83}$) cluster and H-FER zeolites modeled as 64T ($H_{52}Si_{63}(HO)AlO_{101}$) cluster were constructed from the idealized infinite ZSM-5 [44] and FER [45] crystal lattice structures, respectively. The crystal structures of the ZSM-5 and FER respectively cut as 52T and 64T were decorated as following treatment. The dangling bonds of silicon atoms at the edge of 52T ZSM-5 and 64T FER clusters were saturated with hydrogen atoms of which bonds were added along their lattice directions. The next step, all added hydrogen atoms were optimized using AM1 method while the rest atoms are frozen. The acid proton was added by bonding hydrogen atom to one atom of oxygen atoms bridging between the substituted aluminum atom at the crystallographic position T12 on the 52T ZSM-5 cluster for the H-ZSM-5 catalytic model and one atom of two adjacent silicon atoms (T2 on the 64T FER cluster for the H-FER catalyst). The cluster models for the H-ZSM-5 and H-FER catalysts were, therefore, obtained by bonding one proton to oxygen atom which bridges between the T12-Al atom on the ZSM-5 cluster and T2-Al atom on the FER cluster. Double 10T channels for the H-ZSM-5 and H-FER catalysts were taken as the high theoretical zones of which clusters are $H_{10}Si_{21}(HO)AlO_{46}$ and $Si_{19}(HO)AlO_{23}$, respectively. Therefore, the two-layer ONIOM(B3LYP/6-31+G(d,p):AM1) approach for computation modeled are defined as shown in Figure 3.1.

The partial optimizations were employed for all optimized structures, namely all atoms were frozen except atoms labeled with number (see Figure 3.1) were flexible. The molecular fragments Si2-O2-Si1-O1(H1)-Al-O3-Si3-O4-Si4-O5 of the 52T ZSM-5 cluster, Si4-O4-Si3-O3-Si2(O7)-O2-Si1-O1(H1)-Al-(O8)-O5-Si5-O6-Si6 of the 64T FER cluster and all interaction compounds were allowed to move.

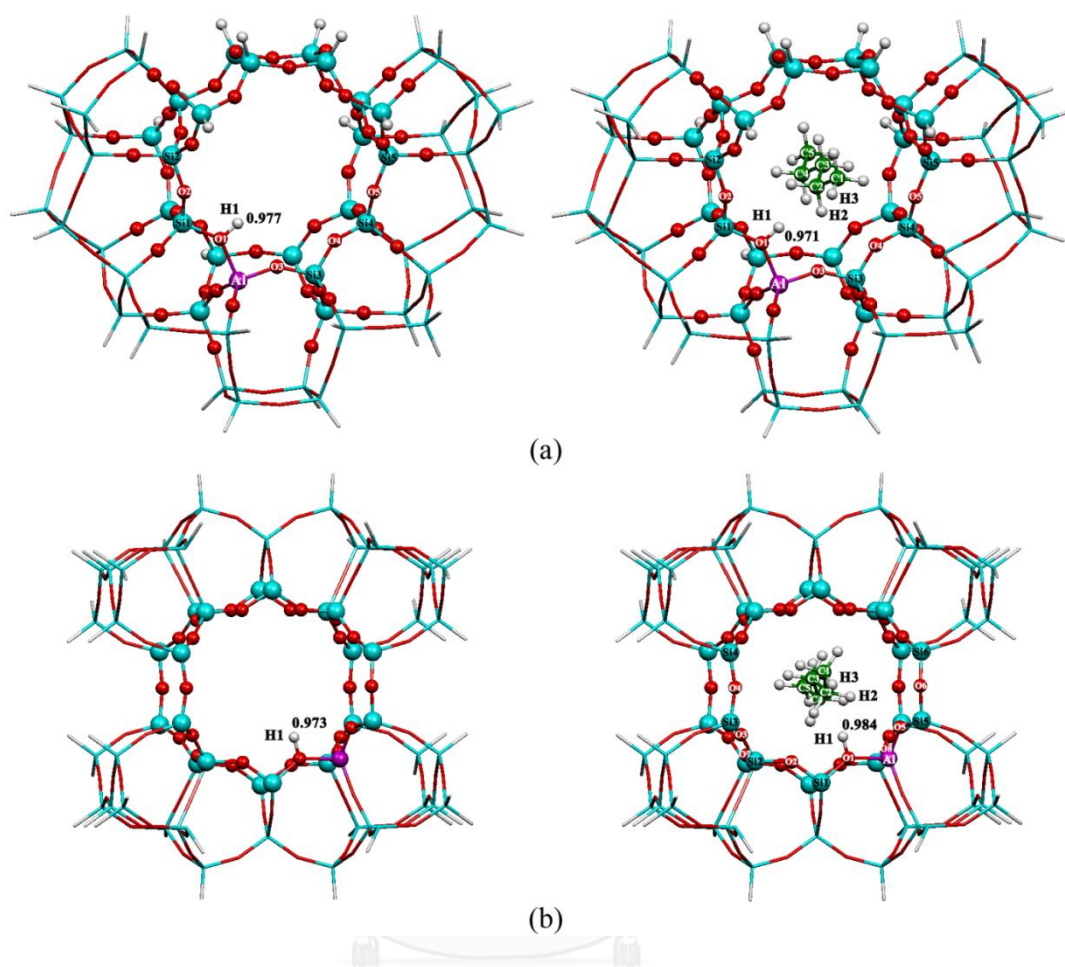


Figure 3.1 The cluster models in combination with the two-layer ONIOM approach for (a) the H-ZSM-5 catalyst (denoted by HZ^{Z}) modeled as the 52T cluster and (b) the H-FER catalyst (denoted by HZ^{F}) modeled as the 64T cluster. The high and low layers defined in the two-layer ONIOM approach are illustrated as the ball and stick atoms, respectively. The molecular images on the righthand side are the optimized structures for their adsorption configuration with the *n*-pentane reactant as representatives.

3.3 Structure optimization and potential energy surface

All the ONIOM(B3LYP/6-31+G(d,p):AM1)-optimized structures except transition-state were confirmed using their vibration mode without imaginary frequency. All the transition-state structures of each cracking reaction step of the *n*-pentane and *n*-hexane over the H-ZSM-5 and H-FER catalyst were obtained and verified by their single imaginary frequency. Relative energies of all related species with the same mass, compared with the sum of total energies of free zeolite cluster and isolated (*n*-pentane and *n*-hexane compounds) reactant were plotted as the potential energy profiles.



CHAPTER IV

RESULTS AND DISCUSSION

The two-layer ONIOM(B3LYP/6-31+G(d,p):AM1)-optimized structures of the H-ZSM-5 and H-FER catalysts which are respectively modeled as 52T and 64T clusters, were obtained as shown in Figure 4.1. The H-O bond lengths of the H-ZSM-5 for HZ^Z (acid proton located at the left side of the Al atom) and Z^ZH (acid proton located at the right side of the Al atom) are respectively 0.977 and 0.977 Å of which stretching vibrations are 3702.4 and 3718.7 cm^{-1} , respectively. These two vibration frequencies are closed to experiments of which stretching vibration is 3740 cm^{-1} [46]. The HZ^Z is more stable than its Z^ZH by 6.17 kcal/mol. The H-O bond lengths of the H-FER for HZ^F (the left acid proton) and Z^FH (the right acid proton) are respectively 0.973 and 0.974 Å of which stretching vibrations are 3760.7 and 3751.3 cm^{-1} , respectively. The HZ^F is more stable than its Z^FH by 1.36 kcal/mol.

4.1 Cracking of *n*-pentane over the H-ZSM-5

The cracking mechanism of *n*-pentane (C_5) over the H-ZSM-5 catalyst consisting of two reaction paths was found. The first path (Path C5_Z^Z , turnover) is the conversion of C_5 to 1,2-pentene (C_5^-) and the second path (Path C5_Z^Z_* , poisoning) is the formation of 2-pentoxy species in ZSM-5. The potential energy profile for *n*-pentane cracking to C_5^- over the H-ZSM-5 catalyst is shown in Figure 4.2. All the ONIOM(B3LYP/6-31+G(d,p):AM1)-optimized structures of the H-ZSM-5 catalyst interacting with related species for the cracking of *n*-pentane over the H-ZSM-5 are shown in Figure 4.3.

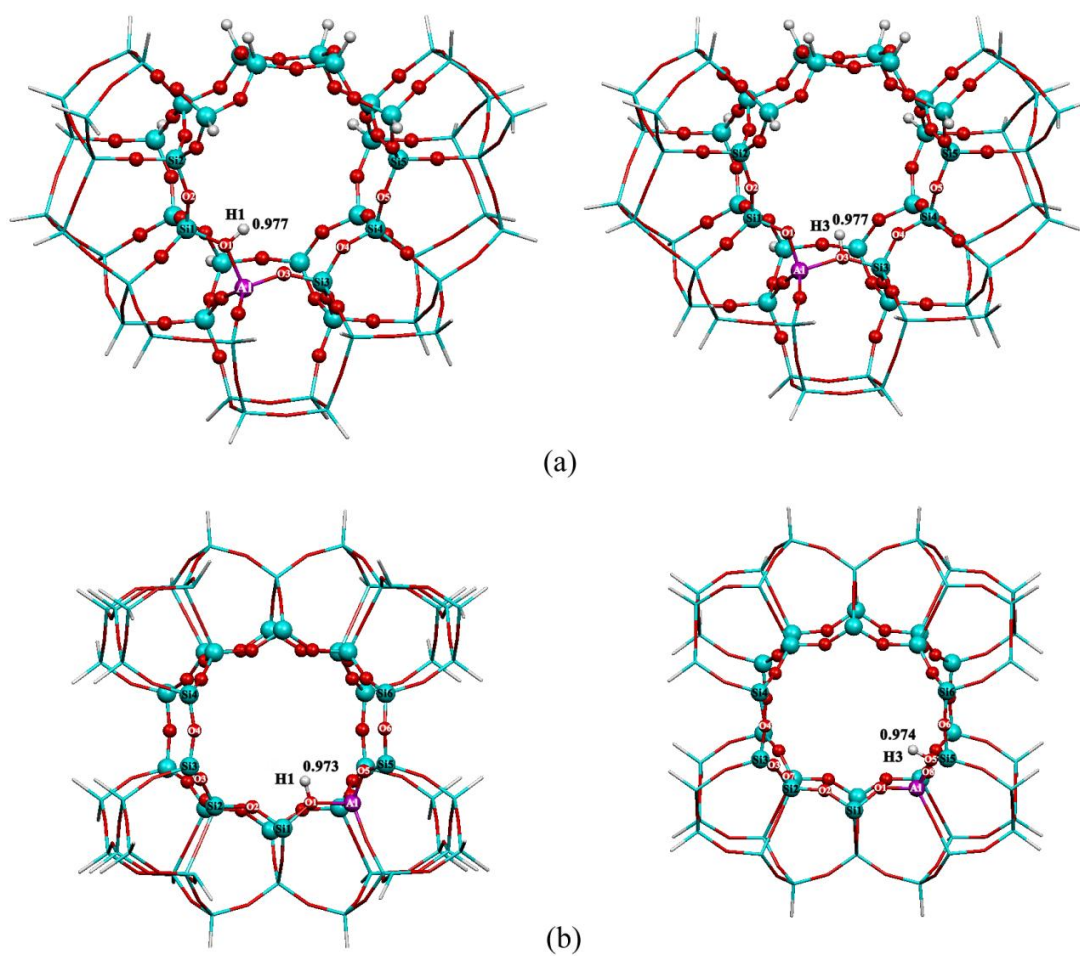


Figure 4.1 The cluster models in combination with the two-layer ONIOM approach for (a) the H-ZSM-5 catalyst modeled as the 52T cluster and (b) the H-FER catalyst modeled as the 64T cluster. The H-O bond lengths are in Å. The stretching vibrations are in cm^{-1} .

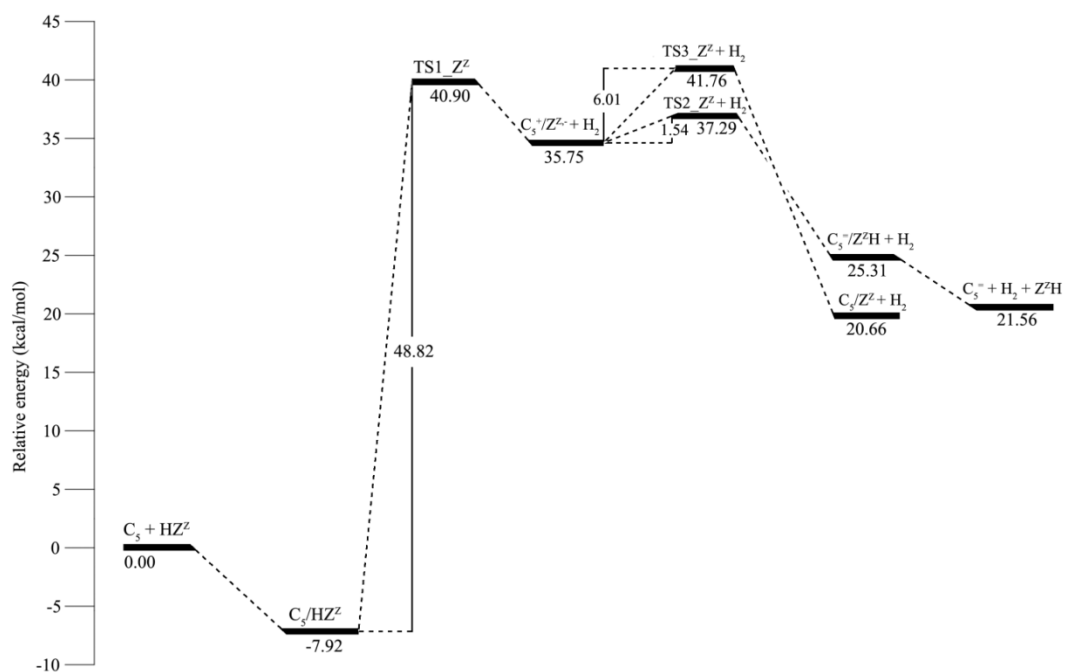


Figure 4.2 Potential energy profile of the Path $C5_Z^Z$ for *n*-pentane (C_5) conversion to 1,2-pentene ($C_5=$) over the H-ZSM-5 (HZ^Z) catalyst.

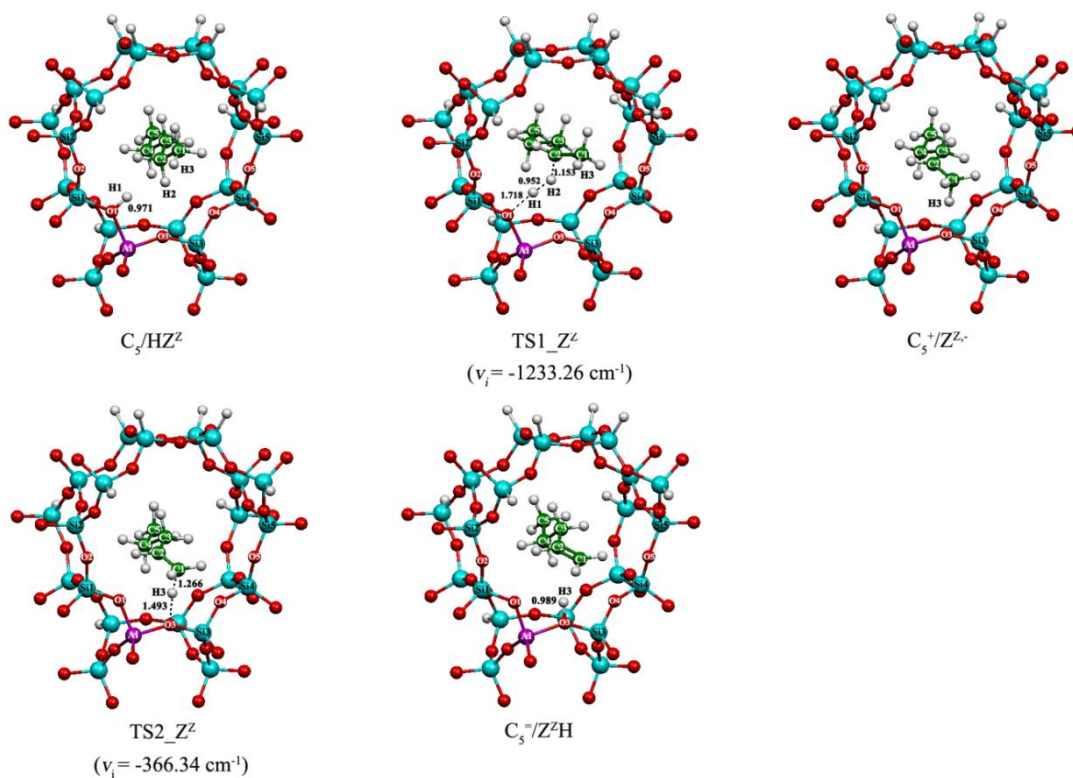


Figure 4.3 The ONIOM(B3LYP/6-31+G(d,p):AM1)-optimized structures of interaction configurations of the H-ZSM-5 with related species in the cracking process of C_5 reactant to $C_5^=$ product. For clarity, portions of their molecular structures are depicted. Bond distances are in Å. The single imaginary frequency for transition-state structures is in parentheses.

The turnover path (Path C5_{Z^Z}) is composed of four reaction steps. The first step, C₅+HZ^Z→C₅/HZ^Z, is adsorption of C₅ on the H-ZSM-5 catalyst (HZ^Z). The second step, C₅/HZ^Z→TS1_{Z^Z}→C₅⁺/Z^{Z-}+H₂, is dehydrogenation reaction taking place via transition state TS1_{Z^Z}. The bond distances between H1 (acid proton) atom of the HZ^Z and H2 atom of C₅ reactant, [H1⋯H2] are of 1.718 and 1.153 Å for the adsorption and transition states, respectively. For the adsorption between C₅⁺/Z^{Z-} species and H₂ molecule, the H1–H2 bond distance of 0.952 Å was found as shown in Figure 4.4. The third step, C₅⁺/Z^{Z-}→TS2_{Z^Z}→C₅⁼/Z^ZH, is the proton–transfer reaction occurring via TS2_{Z^Z} transition state of which the transferring proton bonds to the oxygen atom bridged between right next two silicon atoms; the H-ZSM-5 zeolite is therefore noted by Z^ZH. The transferring proton (H3) detached from C1 atom to bond with O3 of the zeolite; actions of the C1–H3 bond breaking and H3–O3 bond forming simultaneously occurred via TS2_{Z^Z} transition state, as shown in Figure 4.4. The fourth step, C₅⁼/Z^ZH→C₅⁼+Z^ZH, is desorption process to afford C₅⁼ final product. The transition–state structures, TS1_{Z^Z} and TS2_{Z^Z} are confirmed by their single imaginary frequencies, –1233.26 and –366.34 cm⁻¹, respectively as shown in Figure 4.3. The interatomic distances between atoms of the H-ZSM-5 zeolite (HZ^Z) and the interacting species of the turnover path (Path C5_{Z^Z}) of C₅ conversion to C₅⁼ over the H-ZSM-5 zeolite (Z^ZH) are shown in Figure 4.4. The optimized geometrical distances (in Å) between atoms of H-ZSM-5 and interacting species for turnover path (Path C5_{Z^Z}) are showed in Table A-1 of the appendices information.

The reaction energies, thermodynamic properties, rate constants and equilibrium constants for the C₅ cracking over the H-ZSM-5 catalyst are shown in Table 4.1. Related parameters for calculations of the rate constant for turnover path (Path C5_{Z^Z}) are listed in Table A-5. The rate determining step for conversion of the C₅ to C₅⁼, Path C5_{Z^Z} is the second step of which rate constant is 9.52×10⁻²⁵ s⁻¹. The overall equilibrium constant and overall reaction enthalpy for the Path C5_{Z^Z} are 8.92×10⁻¹¹ and 24.51 kcal mol⁻¹, respectively.

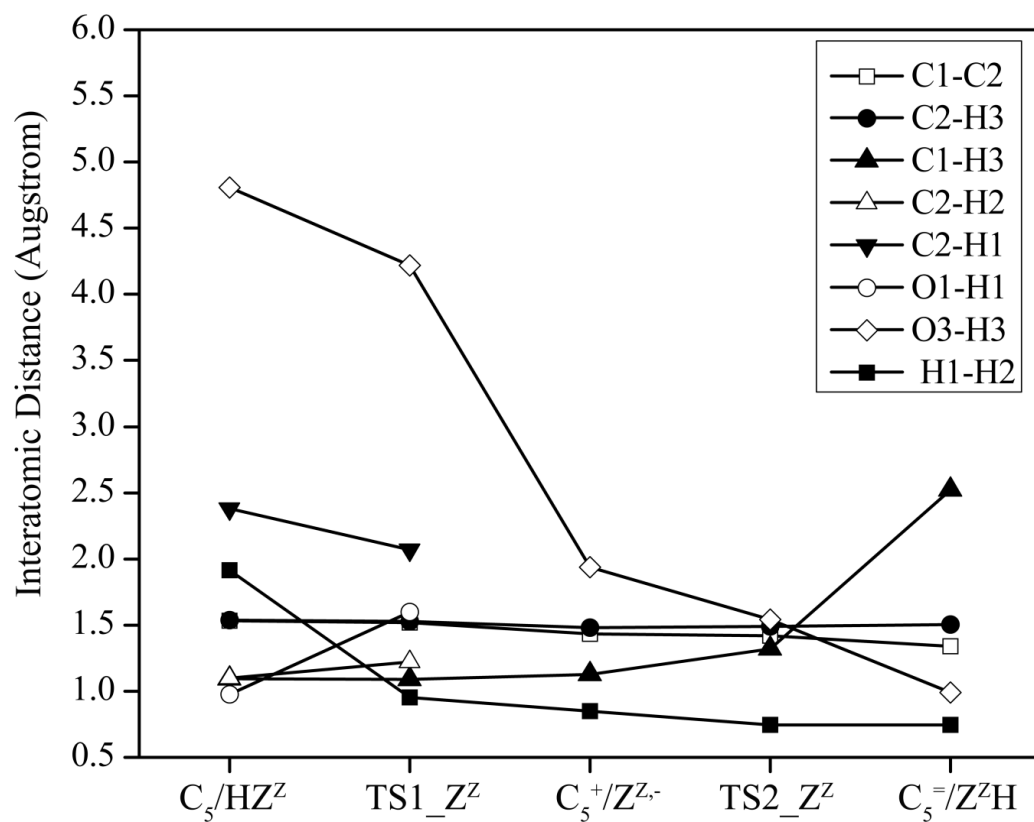


Figure 4.4 Interatomic distances (in Å) between atoms of the H-ZSM-5 (HZ^Z) and interacting species for reaction path (Path $C5_Z^Z$) of C_5 conversion to $C_5^=$ over the H-ZSM-5 catalyst (Z^ZH). Atomic symbols with labels are defined in Figure 3.1.

Table 4.1 Reaction energies, thermodynamic properties, rate and equilibrium constants in the *n*-pentane cracking over the H-ZSM-5 catalyst.

Reaction	$\Delta E^{\ddagger a, b}$	$\Delta G^{\ddagger a, b}$	k_{298}^c	ΔE^a	$\Delta H_{298}^{\circ a}$	$\Delta G_{298}^{\circ a}$	K_{298}
Adsorption							
$C_5+HZ^Z \rightarrow C_5/HZ^Z$	–	–	–	–7.92	–5.98	0.95	2.01×10^{-1}
Progressive conversion							
$C_5/HZ^Z \rightarrow TS1_Z^Z \rightarrow C_5^+/Z^{Z-} + H_2$	48.83	52.01	$9.52 \times 10^{-25, d}$	43.67	46.42	41.61	3.11×10^{-31}
$C_5^+/Z^{Z-} \rightarrow TS2_Z^Z \rightarrow C_5^+/Z^Z H$	1.54	–0.27	1.07×10^{12}	–10.44	–11.62	–13.48	7.67×10^9
Alkoxy species formation ^e							
$C_5^+/Z^{Z-} \rightarrow TS3_Z^Z \rightarrow C_5^+/Z^Z$	6.01	6.15	2.18×10^8	–15.09	–17.07	–16.09	6.25×10^{11}
Desorption							
$C_5^+/Z^Z H \rightarrow C_5^+ + Z^Z H$	–	–	–	–3.75	–4.31	–15.37	1.86×10^{11}

^a Computed at the ONIOM(B3LYP/6-31+G(d,p):AM1) level, in kcal mol⁻¹.

^b Activation energy.

^c In s⁻¹.

^d Rate-determining step.

^e Poisoning path, Path C5_Z^Z_*

The Path C5_Z^Z_* (poisoning path), the three reaction steps was found. The first and second steps of the Path C5_Z^Z_* are common to two initial steps of the Path C5_Z^Z which are the adsorption of C₅ and dehydrogenation of C₅/HZ^Z. The last step, C₅⁺/Z^{Z-} → TS3_Z^Z → C₅⁺Z^Z, is the proton transfer reaction occurring via the TS3_Z^Z transition state to form 2-pentoxy species in ZSM-5. The transition-state structure, TS3_Z^Z is confirmed by its single imaginary frequency, –68.51 cm⁻¹ as shown in Figure 4.5. The overall equilibrium constant and overall reaction enthalpy for Path C5_Z^Z_* are 3.91×10^{-20} and 23.37 kcal mol⁻¹, respectively. It can be concluded that the Path C5_Z^Z is kinetically much more preferred than the Path C5_Z^Z_*. Therefore, the main product for the C₅ cracking on the H-ZSM-5 zeolite is the C₅⁺.

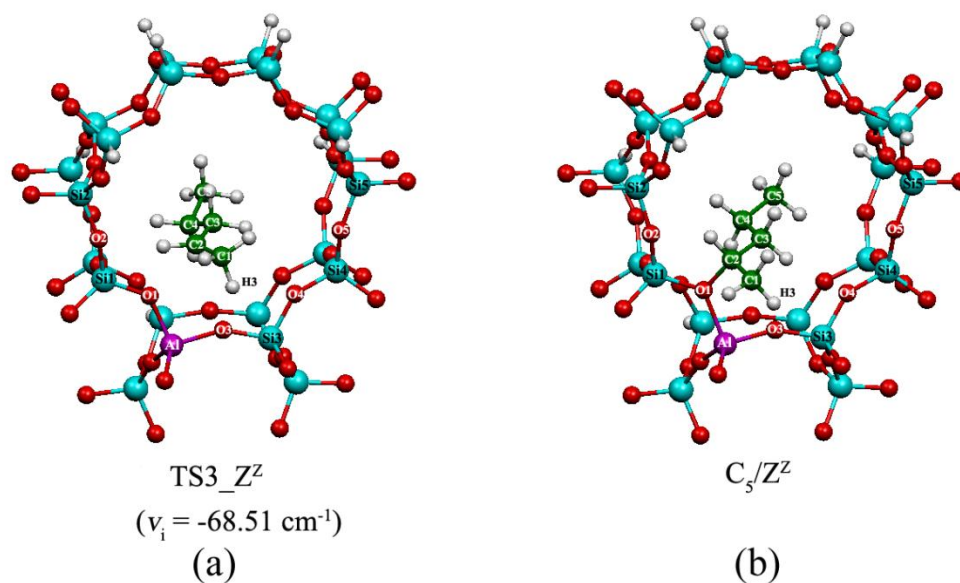


Figure 4.5 The ONIOM(B3LYP/6-31+G(d,p):AM1)-optimized structures of (a) the $TS3_Z^Z$ transition state and (b) 2-pentoxy species on the H-ZSM-5 catalyst. For clarity, portions of the H-ZSM-5 structure are depicted. The single imaginary frequency for transition-state structure is shown in parenthesis.

4.2 Cracking of *n*-hexane over the H-ZSM-5

The cracking mechanism of *n*-hexane (C_6) over the H-ZSM-5 catalyst was also found to consist of two reaction paths. The first path (Path $C6_Z^Z$, turnover) is the conversion of C_6 to 1,2-hexene ($C_6^=$) and the second path (poisoning) is conversion to alkoxy species on the H-ZSM-5, as poisoning. The potential energy profile for the *n*-hexane cracking to $C_6^=$ over the H-ZSM-5 catalyst are shown in Figure 4.6. All the ONIOM(B3LYP/6-31+G(d,p):AM1)-optimized structures involved with C_6 conversion over the H-ZSM-5 catalyst are shown in Figure 4.7.

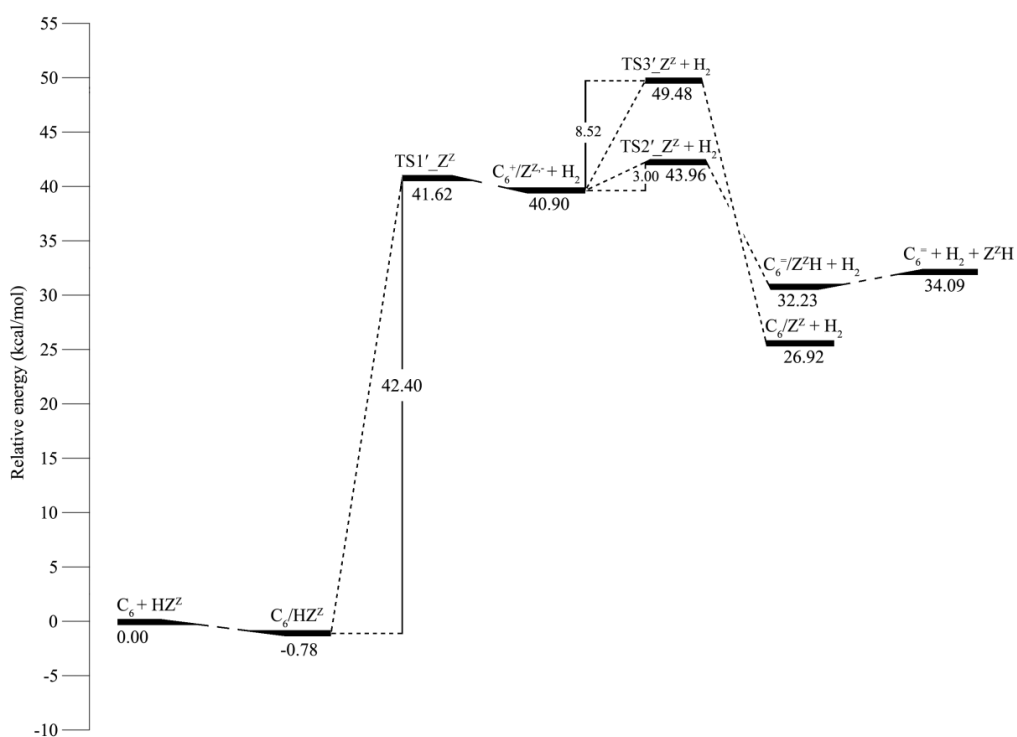


Figure 4.6 Potential energy profile of the Path $C6_ZZ$ for n -hexane (C_6) conversion to 1,2-hexene ($C_6=$) over the H-ZSM-5 (HZZ) catalyst.

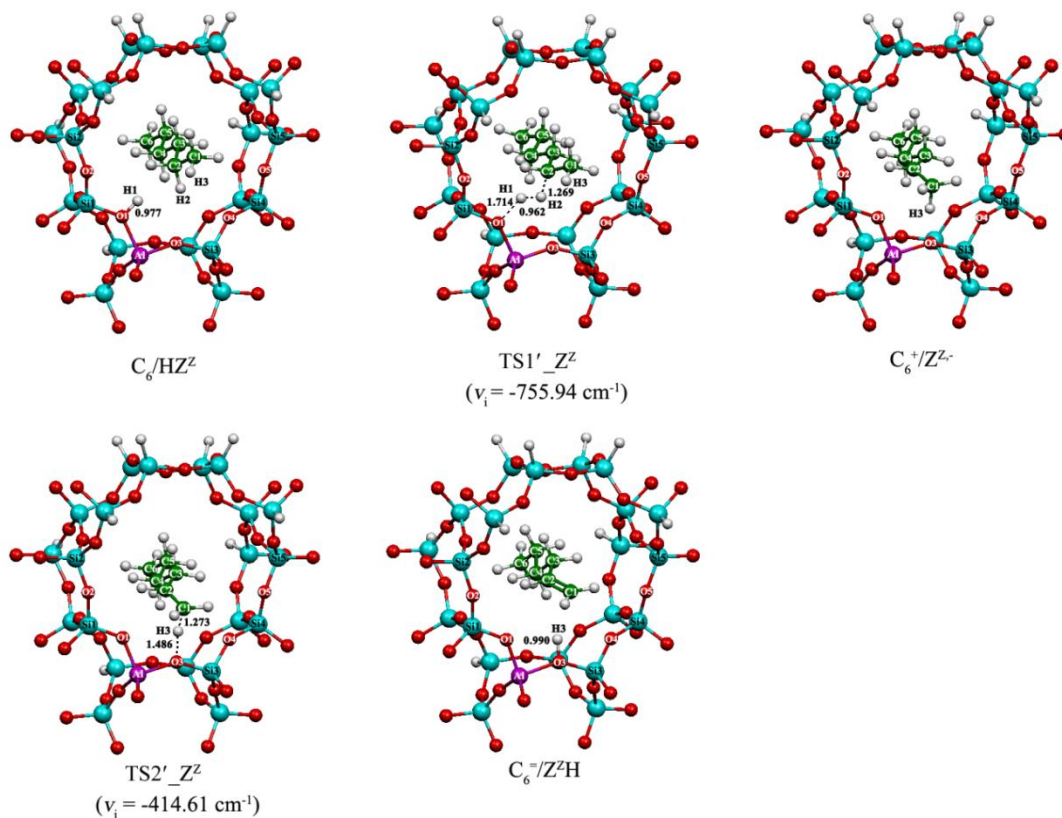


Figure 4.7 The ONIOM(B3LYP/6-31+G(d,p):AM1)-optimized structures of interaction configurations of the H-ZSM-5 with related species in the cracking process of C_6 reactant to C_6^- product. For clarity, portions of their molecular structures are depicted. Bond distances are in Å. The single imaginary frequency for transition-state structures is in parentheses.

The turnover path (Path C6_Z) is composed of four reaction steps. The first step, C₆+HZ^Z→C₆/HZ^Z, is adsorption of C₆ on the H-ZSM-5 catalyst (HZ^Z). The second step, C₆/HZ^Z→TS1'_Z→C₆⁺/Z^{Z-}+H₂, is dehydrogenation reaction taking place via TS1'_Z transition state. The bond distances between H1 (acid proton) atom of the HZ^Z and H2 atom of C₆ reactant, [H1⋯H2] are of 1.714 and 1.269 Å for the adsorption and transition states, respectively. For the adsorption between C₆⁺/Z^{Z-} species and H₂ molecule, the H1–H2 bond distance of 0.962 Å was found as shown in Figure 4.8. The third step, C₆⁺/Z^{Z-}→TS2'_Z→C₆⁼/Z^ZH, is the proton-transfer reaction occurring via transition state TS2'_Z of which the transferring proton bonds to the oxygen atom bridged between right next two silicon atoms; the H-ZSM-5 zeolite is therefore noted by Z^ZH. The transferring proton (H3) detached from C1 atom to bond with O3 of the zeolite; actions of the C1–H3 bond breaking and H3–O3 bond forming simultaneously occurred via transition state TS2'_Z, as shown in Figure 4.8. The fourth step, C₆⁼/Z^ZH→C₆⁼+Z^ZH, is desorption process to afford C₆⁼ final product. The transition-state structures, TS1'_Z and TS2'_Z are confirmed by their single imaginary frequencies, -755.94 and -414.61 cm⁻¹, respectively as shown in Figure 4.7. The interatomic distances between atoms of the H-ZSM-5 zeolite (HZ^Z) and the interacting species of the turnover path (Path C6_Z) of C₆ conversion to C₆⁼ over the H-ZSM-5 zeolite (Z^ZH) are shown in Figure 4.8. The optimized geometrical distances (in Å) between atoms of H-ZSM-5 and interacting species for turnover path (Path C6_Z) are showed in Table A-2 of the appendices information.

The reaction energies, thermodynamic properties, rate constants and equilibrium constants for the C₆ cracking over the H-ZSM-5 catalyst are shown in Table 4.2. Related parameters for calculations of the rate constant for turnover path (Path C6_Z) are listed in Table A-6. The rate determining step for conversion of the C₆ to C₆⁼, Path C6_Z is the second step of which rate constant is 5.15×10⁻²⁰ s⁻¹. The overall equilibrium constant and overall reaction enthalpy for the Path C6_Z are 1.30×10⁻²⁰ and 35.83 kcal mol⁻¹, respectively.

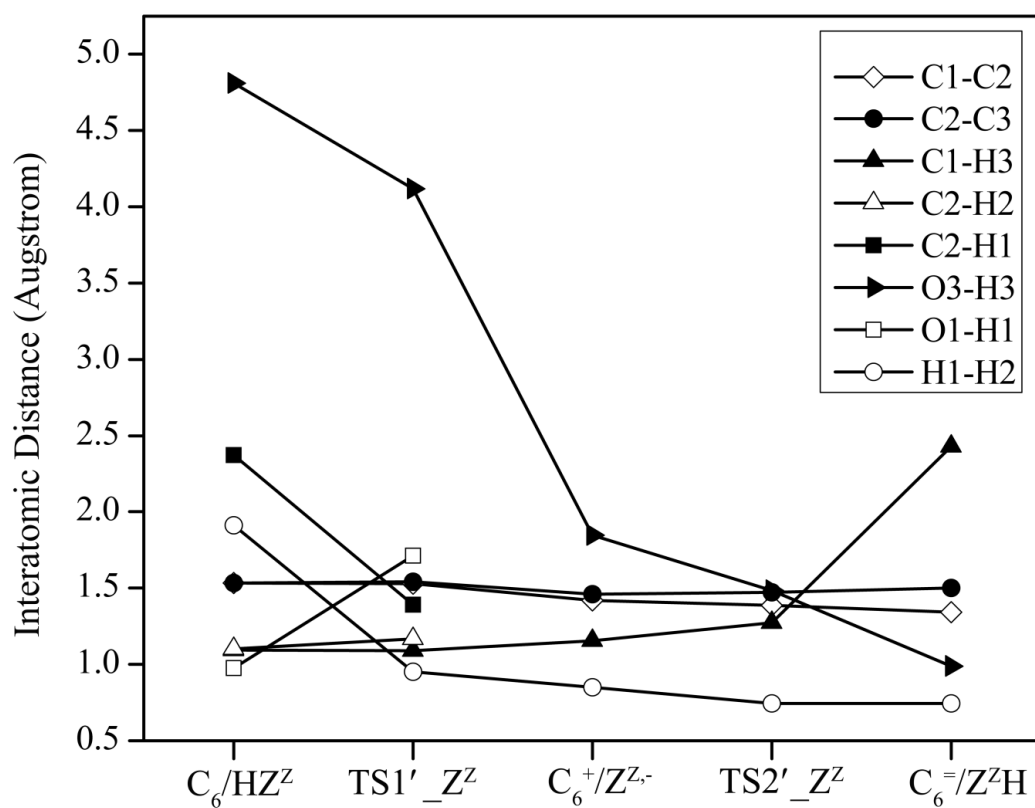


Figure 4.8 Interatomic distances (in Å) between atoms of the H-ZSM-5 (HZ^Z) and interacting species for reaction path (Path $C6_Z^Z$) of C_6 conversion to $C_6^=$ over the H-ZSM-5 catalyst (Z^ZH). Atomic symbols with labels are defined in Figure 3.1.

Table 4.2 Reaction energies, thermodynamic properties, rate and equilibrium constants in the *n*-hexane cracking over the H-ZSM-5 catalyst.

Reaction	$\Delta E^{\ddagger a,b}$	$\Delta G^{\ddagger a,b}$	k_{298}^c	ΔE^a	$\Delta H_{298}^O^a$	$\Delta G_{298}^O^a$	K_{298}
Adsorption							
$C_6+HZ^Z \rightarrow C_6/HZ^Z$	-	-	-	-0.78	-0.07	10.73	1.37×10^{-8}
Progressive conversion							
$C_6/HZ^Z \rightarrow TS1'_Z^Z \rightarrow C_6^+/Z^{Z-} + H_2$	42.39	44.02	$5.15 \times 10^{-20,d}$	41.73	46.48	36.53	1.66×10^{-27}
$C_6^+/Z^{Z-} \rightarrow TS2'_Z^Z \rightarrow C_6^=/Z^ZH$	3.01	3.23	1.09×10^{10}	-8.72	-11.97	-9.60	1.10×10^7
Alkoxy species formation^e							
$C_6^+/Z^{Z-} \rightarrow TS3'_Z^Z \rightarrow C_6^Z^Z$	8.52	9.41	4.14×10^5	-14.03	-18.03	-12.92	2.98×10^9
Desorption							
$C_6^=/Z^ZH \rightarrow C_6^= + Z^ZH$	-	-	-	1.86	1.39	-10.53	5.21×10^7

^a Computed at the ONIOM(B3LYP/6-31+G(d,p):AM1) level, in kcal mol⁻¹.

^b Activation energy.

^c In s⁻¹.

^d Rate-determining step.

^e Poisoning path, Path C6_Z^Z_*.

The Path C6_Z^Z_* (poisoning path), the three reaction steps was found. The first and second steps of the Path C6_Z^Z_* are common to two initial steps of the Path C6_Z^Z which are the adsorption of C₆ and dehydrogenation of C₆/HZ^Z. The last step, C₆⁺/Z^{Z-} → TS3'_Z^Z → C₆⁼Z^Z, is the proton transfer reaction occurring via the transition state TS3'_Z^Z to form 2-hexoxy species in ZSM-5. The transition-state structure, TS3'_Z^Z is confirmed by its single imaginary frequency, -83.88 cm⁻¹ as shown in Figure 4.9. The overall equilibrium constant and overall reaction enthalpy for Path C6_Z^Z_* are 6.78×10^{-26} and 28.38 kcal mol⁻¹, respectively. It can be concluded that the Path C6_Z^Z is kinetically much more preferred than the Path C6_Z^Z_*. Therefore, the main product for the C₆ cracking on the H-ZSM-5 zeolite is the C₆⁼.

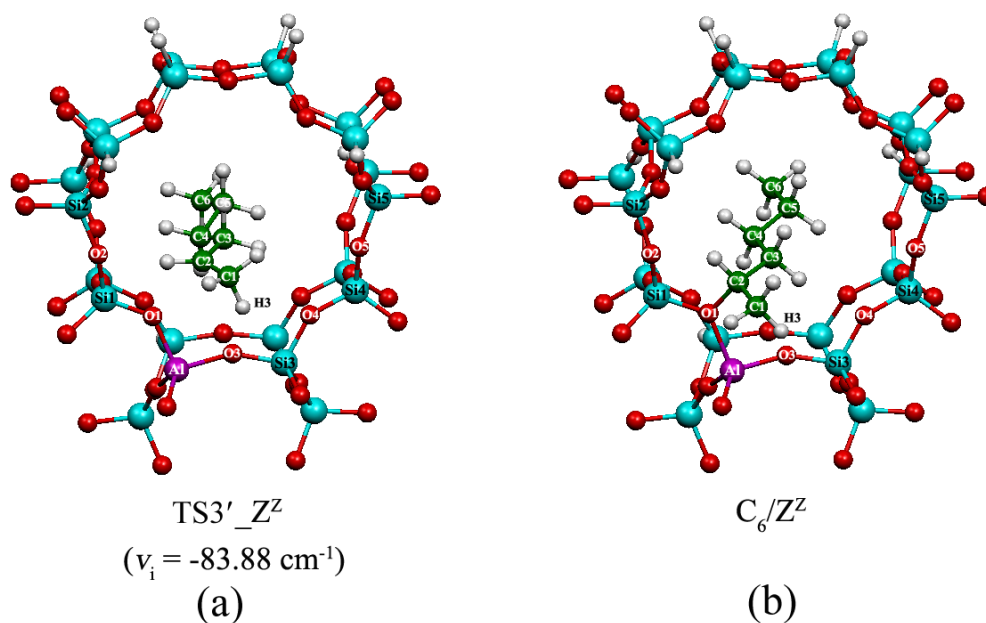


Figure 4.9 The ONIOM(B3LYP/6-31+G(d,p):AM1)-optimized structures of (a) the $\text{TS3}_{\text{Z}}^{\text{Z}}$ transition state and (b) 2-hexoxy species on the H-ZSM-5 catalyst. For clarity, portions of the H-ZSM-5 structure are depicted. The single imaginary frequency for transition-state structure is shown in parenthesis.

4.3 Cracking of *n*-pentane over the H-FER

The cracking mechanism of *n*-pentane (C_5) over the H-FER catalyst consisting of two reaction paths was found. The first path (Path $\text{C5}_{\text{Z}}^{\text{F}}$, turnover) is the conversion of C_5 to 1,2-pentene (C_5^{F}) and the second path (Path $\text{C5}_{\text{Z}}^{\text{F}*}$, poisoning) is the formation of 2-pentoxy species in FER. The potential energy profile for *n*-pentane cracking to C_5^{F} over the H-FER catalyst is shown in Figure 4.10. All the ONIOM(B3LYP/6-31+G(d,p):AM1)-optimized structures of the H-FER catalyst interacting with related species for the cracking of *n*-pentane over the H-FER are shown in Figure 4.11.

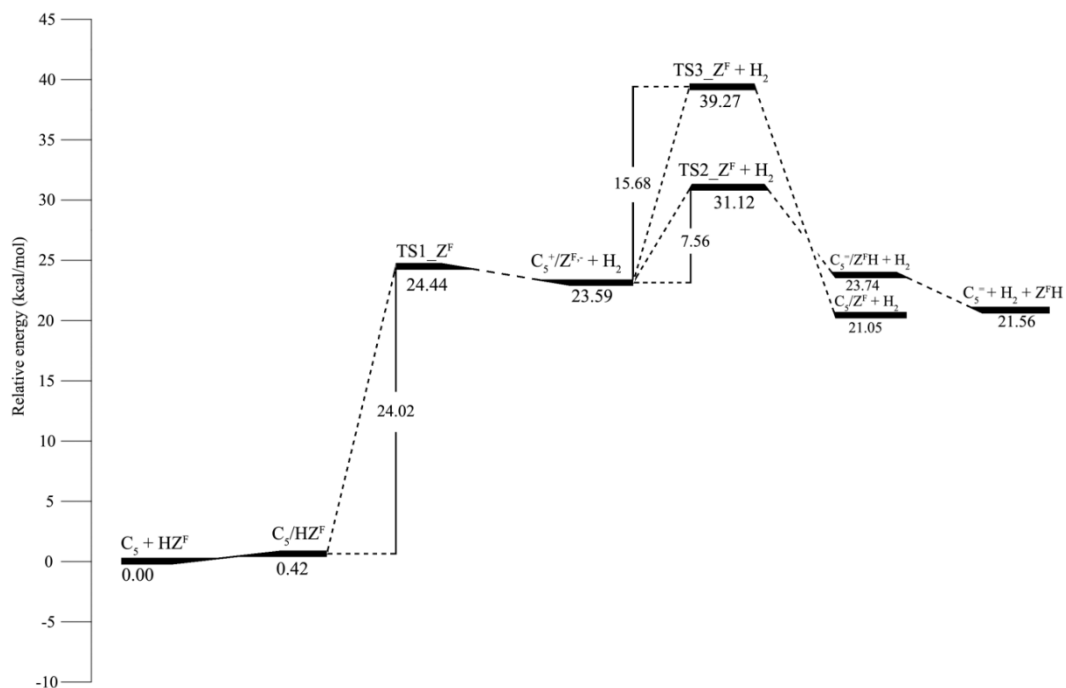


Figure 4.10 Potential energy profile of the Path $C5_Z^F$ for *n*-pentane (C_5) conversion to 1,2-pentene (C_5^-) over the H-FER (HZ^F) catalyst.

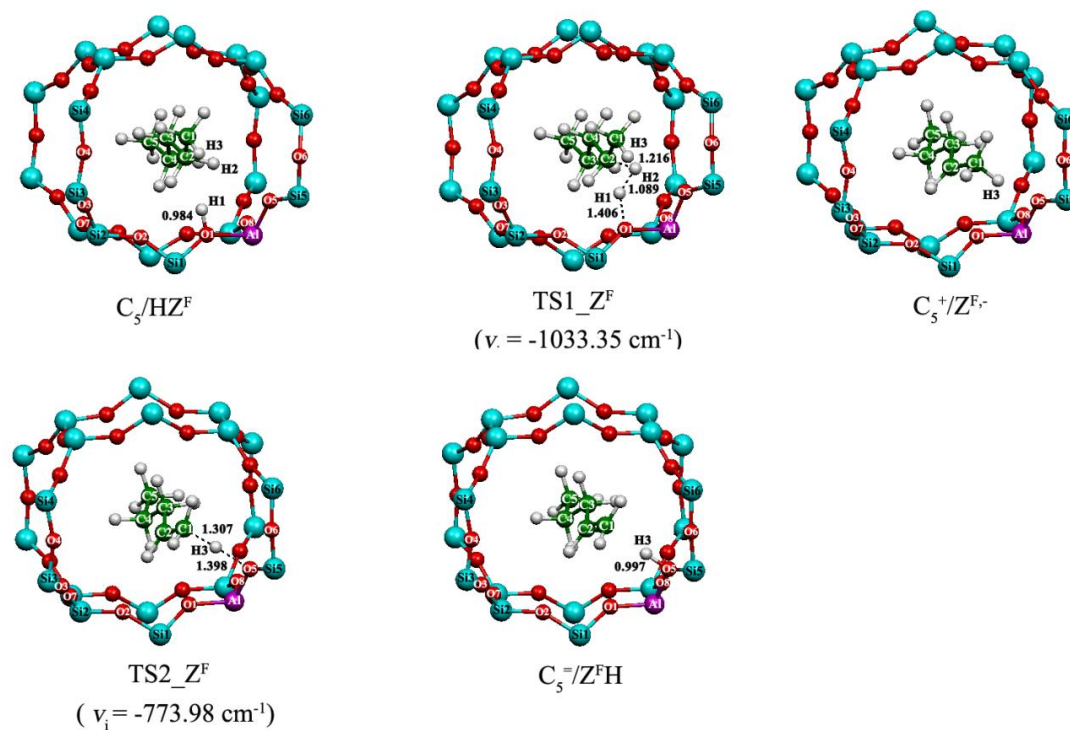


Figure 4.11 The ONIOM(B3LYP/6-31+G(d,p):AM1)-optimized structures of interaction configurations of the H-FER with related species in the cracking process of C_5 reactant to C_5^- product. For clarity, portions of their molecular structures are depicted. Bond distances are in Å. The single imaginary frequency for transition-state structures is in parentheses.

The turnover path (Path C5_{Z^F}) is composed of four reaction steps. The first step, C₅+HZ^F→C₅/HZ^F, is adsorption of C₅ on the H-FER catalyst (HZ^F). The second step, C₅/HZ^F→TS1_{Z^F}→C₅⁺/Z^{F,-}+H₂, is dehydrogenation reaction taking place via TS1_{Z^F} transition state. The bond distances between H1 (acid proton) atom of the HZ^F and H2 atom of C₅ reactant, [H1···H2] are of 1.406 and 1.216 Å for the adsorption and transition states, respectively. For the adsorption between C₅⁺/Z^{F,-} species and H₂ molecule, the H1–H2 bond distance of 1.089 Å was found as shown in Figure 4.12. The third step, C₅⁺/Z^{F,-}→TS2_{Z^F}→C₅⁼/Z^FH, is the proton-transfer reaction occurring via TS2_{Z^F} transition state of which the transferring proton bonds to the oxygen atom bridged between right next two silicon atoms; the H-FER zeolite is therefore noted by Z^FH. The transferring proton (H3) detached from C1 atom to bond with O5 of the zeolite; actions of the C1–H3 bond breaking and H3–O5 bond forming simultaneously occurred via TS2_{Z^F} transition state, as shown in Figure 4.12. The fourth step, C₅⁼/Z^FH→C₅⁼+Z^FH, is desorption process to afford C₅⁼ final product. The transition-state structures, TS1_{Z^F} and TS2_{Z^F} are confirmed by their single imaginary frequencies, -1033.35 and -773.98 cm⁻¹, respectively as shown in Figure 4.11. The interatomic distances between atoms of the H-FER zeolite (HZ^Z) and the interacting species of the turnover path (Path C5_{Z^F}) of C₅ conversion to C₅⁼ over the H-FER zeolite (Z^FH) are shown in Figure 4.12. The optimized geometrical distances (in Å) between atoms of H-FER and interacting species for turnover path (Path C5_{Z^F}) are showed in Table A-3 of the appendices information.

The reaction energies, thermodynamic properties, rate constants and equilibrium constants for the C₅ cracking over the H-FER catalyst are shown in Table 4.3. Related parameters for calculations of the rate constant for turnover path (Path C5_{Z^F}) are listed in Table A-7. The rate determining step for conversion of the C₅ to C₅⁼, Path C5_{Z^F} is the second step of which rate constant is 4.12×10⁻⁶ s⁻¹. The overall equilibrium constant and overall reaction enthalpy for the Path C5_{Z^F} are 8.92×10⁻¹¹ and 24.50 kcal mol⁻¹, respectively.

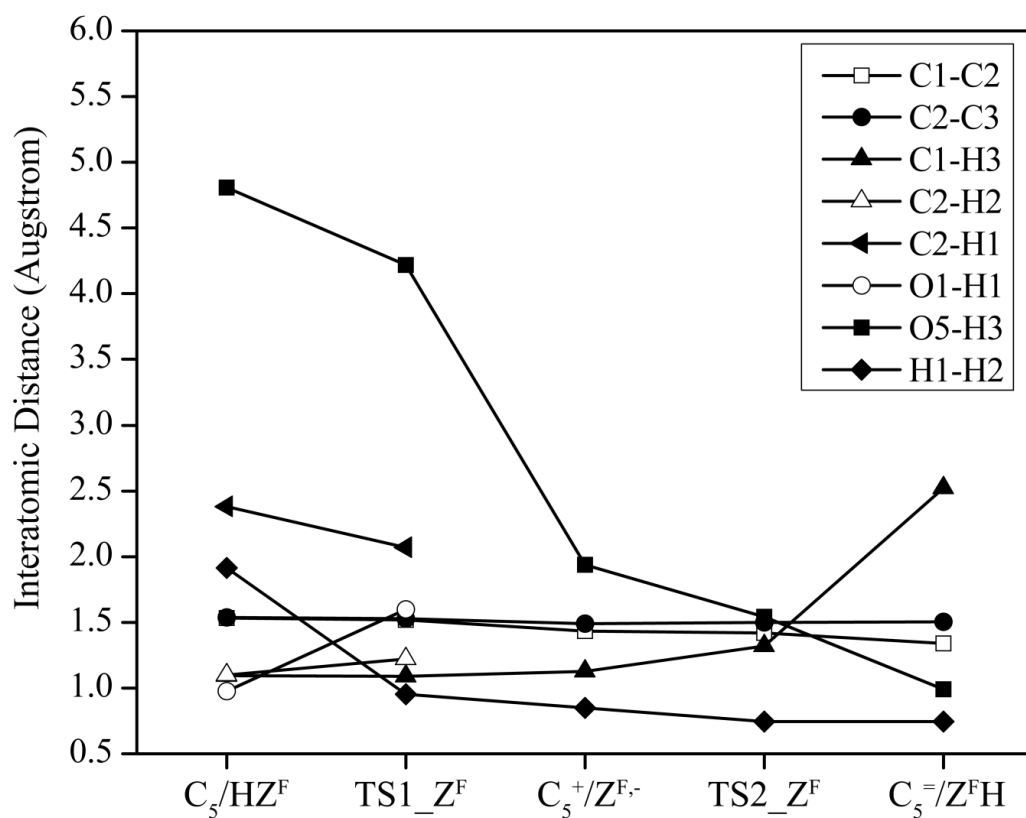


Figure 4.12 Interatomic distances (in Å) between atoms of the H-FER (HZ^F) and interacting species for reaction path (Path C5_Z^F) of C₅ conversion to C₅⁼ over the H-FER catalyst (Z^FH). Atomic symbols with labels are defined in Figure 3.1.

Table 4.3 Reaction energies, thermodynamic properties, rate and equilibrium constants in the *n*-pentane cracking over the H-FER catalyst.

Reaction	$\Delta E^{\ddagger a,b}$	$\Delta G^{\ddagger a,b}$	k_{298}^c	ΔE^a	$\Delta H_{298}^O^a$	$\Delta G_{298}^O^a$	K_{298}
Adsorption							
$C_5 + HZ^F \rightarrow C_5/HZ^F$	–	–	–	0.42	1.98	12.00	1.60×10^{-9}
Progressive conversion							
$C_5/HZ^F \rightarrow TS1_Z^F \rightarrow C_5^+/Z^{F,-} + H_2$	24.02	24.83	$4.12 \times 10^{-6,d}$	23.17	31.67	17.09	2.95×10^{-13}
$C_5^+/Z^{F,-} \rightarrow TS2_Z^F \rightarrow C_5^=/Z^FH$	7.52	8.22	3.20×10^6	0.15	-6.93	-0.38	1.89×10^0
Alkoxy species formation^e							
$C_5^+/Z^{F,-} \rightarrow TS3_Z^F \rightarrow C_5/Z^F$	15.68	15.72	1.69×10^1	-2.51	-10.23	-0.98	5.24×10^0
Desorption							
$C_5^=/Z^FH \rightarrow C_5^- + Z^FH$	–	–	–	-2.18	-2.22	-15.01	1.00×10^{11}

^a Computed at the ONIOM(B3LYP/6-31+G(d,p):AM1) level, in kcal mol⁻¹.

^b Activation energy.

^c In s⁻¹.

^d Rate-determining step.

^e Poisoning path, Path C5_Z^F_*

The Path C5_Z^F_* (poisoning path), the three reaction steps was found. The first and second steps of the Path C5_Z^F_* are common to two initial steps of the Path C5_Z^F which are the adsorption of C₅ and dehydrogenation of C₅/HZ^F. The last step, C₅⁺/Z^{F,-} → TS3_Z^F → C₅Z^F, is the proton transfer reaction occurring via the TS3_Z^F transition state to form 2-pentoxy species in FER. The transition-state structure, TS3_Z^F is confirmed by its single imaginary frequency, -105.49 cm⁻¹ as shown in Figure 4.13. The overall equilibrium constant and overall reaction enthalpy for Path C5_Z^F_* are 2.47×10^{-21} and 23.42 kcal mol⁻¹, respectively. It can be concluded that the Path C5_Z^F is kinetically much more preferred than the Path C5_Z^F_*. Therefore, the main product for the C₅ cracking on the H-FER zeolite is the C₅⁼.

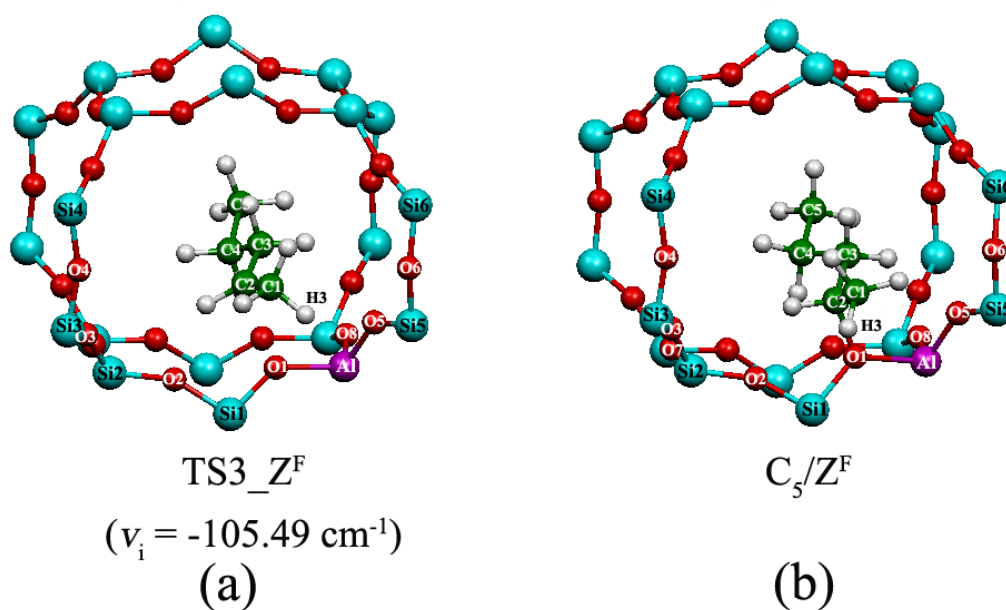


Figure 4.13 The ONIOM(B3LYP/6-31+G(d,p):AM1)-optimized structures of (a) the TS3_Z^{F} transition state and (b) 2-pentoxy species on the H-FER catalyst. For clarity, portions of the H-FER structure are depicted. The single imaginary frequency for transition-state structure is shown in parenthesis.

4.4 Cracking of *n*-hexane over the H-FER

The cracking mechanism of *n*-hexane (C_6) over the H-FER catalyst consisting of two reaction paths was found. The first path (Path C6_Z^{F} , turnover) is the conversion of C_5 to 1,2-hexene ($\text{C}_6^{\text{=}}$) and the second path (Path $\text{C6_Z}^{\text{F}*}$, poisoning) is the formation of 2-hexoxy species in FER. The potential energy profile for *n*-hexane cracking to $\text{C}_6^{\text{=}}$ over the H-FER catalyst is shown in Figure 4.14. All the ONIOM(B3LYP/6-31+G(d,p):AM1)-optimized structures of the H-FER catalyst interacting with related species for the cracking of *n*-hexane over the H-FER are shown in Figure 4.15.

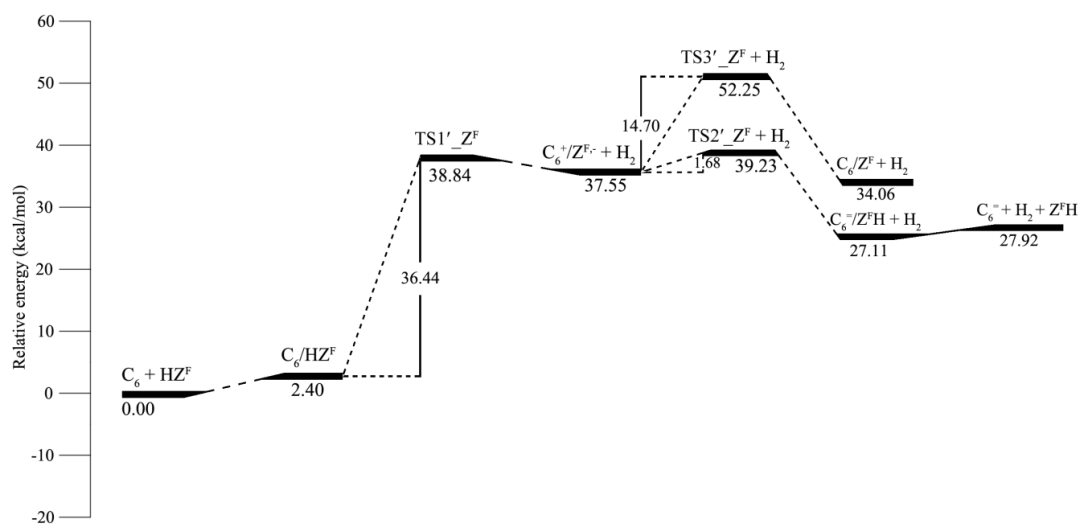
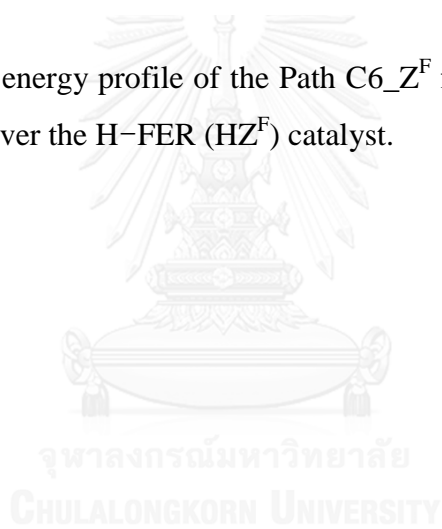


Figure 4.14 Potential energy profile of the Path $C6_Z^F$ for n -hexane (C_6) conversion to 1,2-hexene (C_6^-) over the H-FER (HZ^F) catalyst.



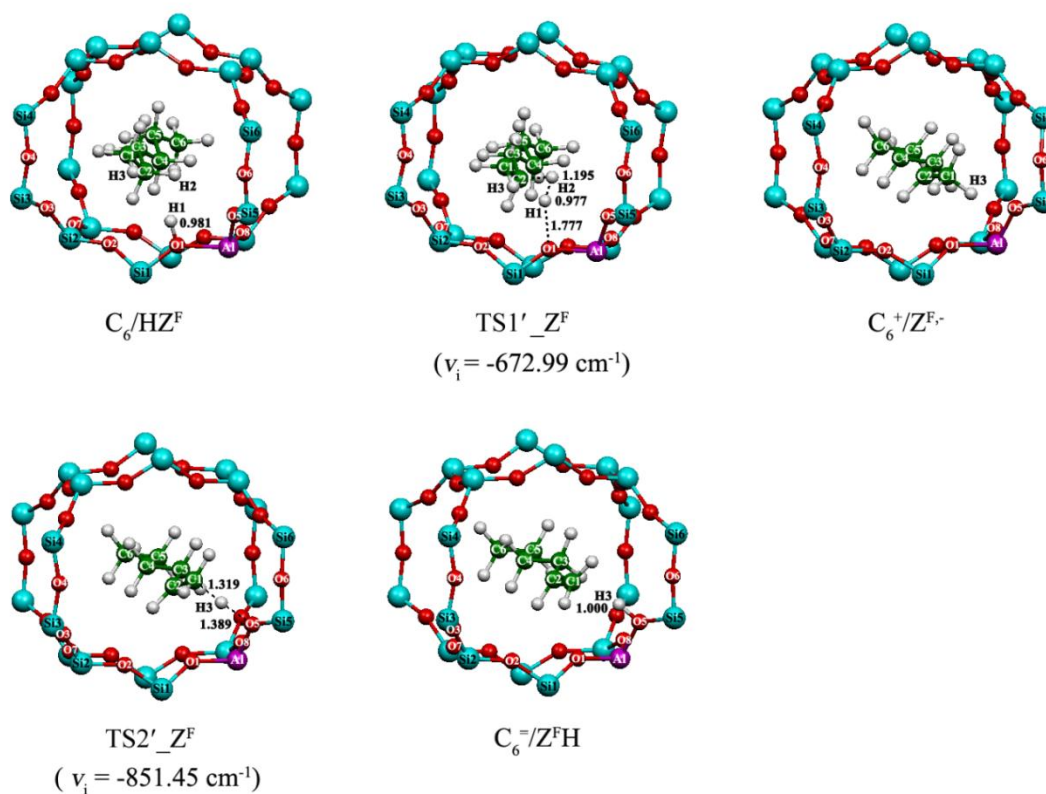


Figure 4.15 The ONIOM(B3LYP/6-31+G(d,p):AM1)-optimized structures of interaction configurations of the H-FER with related species in the cracking process of C_6 reactant to C_6^- product. For clarity, portions of their molecular structures are depicted. Bond distances are in Å. The single imaginary frequency for transition-state structures is in parentheses.

The turnover path (Path C6_{Z^F}) is composed of four reaction steps. The first step, C₆+HZ^F→C₆/HZ^F, is adsorption of C₆ on the H-FER catalyst (HZ^F). The second step, C₆/HZ^F→TS1'_{Z^F}→C₆⁺/Z^{F,-}+H₂, is dehydrogenation reaction taking place via TS1'_{Z^F} transition state. The bond distances between H1 (acid proton) atom of the HZ^F and H2 atom of C₆ reactant, [H1···H2] are of 1.777 and 1.195 Å for the adsorption and transition states, respectively. For the adsorption between C₆⁺/Z^{F,-} species and H₂ molecule, the H1–H2 bond distance of 0.977 Å was found as shown in Figure 4.16. The third step, C₆⁺/Z^{F,-}→TS2'_{Z^F}→C₆⁼/Z^FH, is the proton-transfer reaction occurring via TS2'_{Z^F} transition state of which the transferring proton bonds to the oxygen atom bridged between right next two silicon atoms; the H-FER zeolite is therefore noted by Z^FH. The transferring proton (H3) detached from C1 atom to bond with O5 of the zeolite; actions of the C1–H3 bond breaking and H3–O5 bond forming simultaneously occurred via TS2'_{Z^F} transition state, as shown in Figure 4.16. The fourth step, C₆⁼/Z^FH→C₆⁼+Z^FH, is desorption process to afford C₆⁼ final product. The transition-state structures, TS1'_{Z^F} and TS2'_{Z^F} are confirmed by their single imaginary frequencies, -672.99 and -851.45 cm⁻¹, respectively as shown in Figure 4.15. The interatomic distances between atoms of the H-FER zeolite (HZ^Z) and the interacting species of the turnover path (Path C6_{Z^F}) of C₆ conversion to C₆⁼ over the H-FER zeolite (Z^FH) are shown in Figure 4.16. The Optimized geometrical distances (in Å) between atoms of H-FER and interacting species for turnover path (Path C6_{Z^F}) are showed in Table A-4 of the appendices information.

The reaction energies, thermodynamic properties, rate constants and equilibrium constants for the C₆ cracking over the H-FER catalyst are shown in Table 4.4. Related parameters for calculations of the rate constant for turnover path (Path C6_{Z^F}) are listed in Table A-8. The rate determining step for conversion of the C₆ to C₆⁼, Path C6_{Z^F} is the second step of which rate constant is 1.94×10⁻¹⁵ s⁻¹. The overall equilibrium constant and overall reaction enthalpy for the Path C6_{Z^F} are 4.45×10⁻¹⁶ and 29.69 kcal mol⁻¹, respectively.

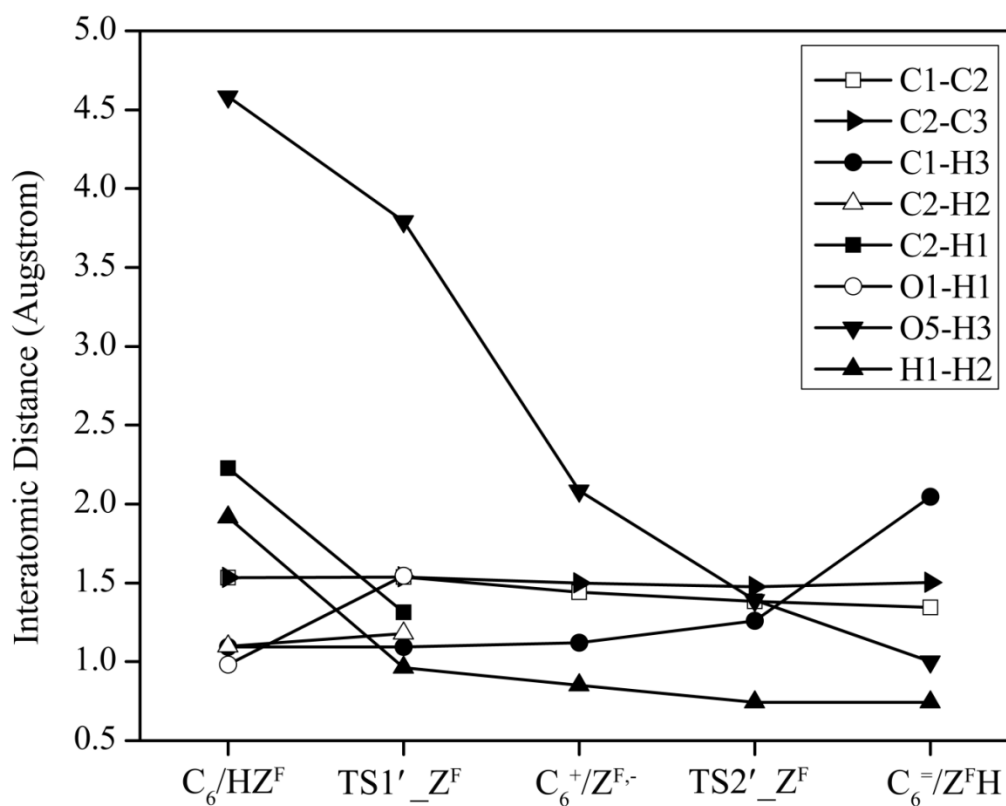


Figure 4.16 Interatomic distances (in Å) between atoms of the H-FER (HZ^F) and interacting species for reaction path (Path $C6_Z^F$) of C_6 conversion to $C_6^=$ over the H-FER catalyst (Z^FH). Atomic symbols with labels are defined in Figure 3.1.

Table 4.4 Reaction energies, thermodynamic properties, rate and equilibrium constants in the *n*-hexane cracking over the H-FER catalyst.

Conversion reaction	$\Delta E^{\ddagger a,b}$	$\Delta G^{\ddagger a,b}$	k_{298}^c	ΔE^a	$\Delta H_{298}^{\circ a}$	$\Delta G_{298}^{\circ a}$	K_{298}
Adsorption							
$C_6 + HZ^F \rightarrow C_6/HZ^F$	–	–	–	2.40	9.05	15.33	5.82×10^{-12}
Progressive conversion							
$C_6/HZ^F \rightarrow TS1'_Z^F \rightarrow C_6^+/Z^{F,-} + H_2$	36.44	37.71	$1.94 \times 10^{-15,d}$	35.15	30.41	29.24	3.67×10^{-22}
$C_6^+/Z^{F,-} \rightarrow TS2'_Z^F \rightarrow C_6^-/Z^FH$	1.68	2.37	1.93×10^{11}	-10.43	-10.02	-12.26	9.69×10^8
Alkoxy species formation^e							
$C_6^+/Z^{F,-} \rightarrow TS3'_Z^F \rightarrow C_6^F$	14.70	16.98	2.23×10^0	-3.49	-4.28	-2.05	3.17×10^1
Desorption							
$C_6^-/Z^FH \rightarrow C_6^- + Z^FH$	–	–	–	0.81	0.25	-11.37	2.15×10^8

^a Computed at the ONIOM(B3LYP/6-31+G(d,p):AM1) level, in kcal mol⁻¹.

^b Activation energy.

^c In s⁻¹.

^d Rate-determining step.

^e Poisoning path, Path C6_Z^F_*

The Path C6_Z^F_* (poisoning path), the three reaction steps was found. The first and second steps of the Path C6_Z^F_* are common to two initial steps of the Path C6_Z^F which are the adsorption of C₆ and dehydrogenation of C₆/HZ^F. The last step, C₆⁺/Z^{F,-} → TS3'_Z^F → C₆^F, is the proton transfer reaction occurring via the TS3'_Z^F transition state to form 2-hexoxy species in FER. The transition-state structure, TS3'_Z^F is confirmed by its single imaginary frequency, -126.49 cm⁻¹ as shown in Figure 4.17. The overall equilibrium constant and overall reaction enthalpy for Path C6_Z^F_* are 6.77×10^{-32} and 35.18 kcal mol⁻¹, respectively. It can be concluded that the Path C6_Z^F is kinetically much more preferred than the Path C6_Z^F_* and the main product for the C₆ cracking on the H-FER zeolite is therefore the C₆⁻.

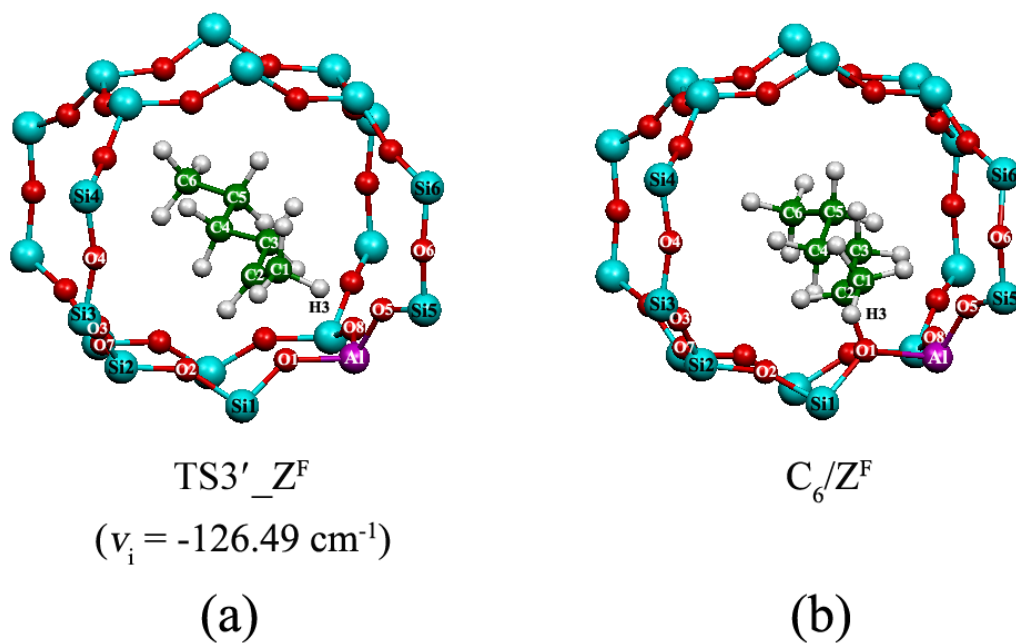


Figure 4.17 The ONIOM(B3LYP/6-31+G(d,p):AM1)-optimized structures of (a) the TS3_Z^F transition state and (b) 2-hexoxy species on the H-FER catalyst. For clarity, portions of the H-FER structure are depicted. The single imaginary frequency for transition-state structure is shown in parenthesis.

CHAPTER V

CONCLUSION

The cracking reactions of *n*-pentane and *n*-hexane over the H-ZSM-5 and H-FER catalysts were theoretically investigated using the two-layer ONIOM(B3LYP/6-31+G(d,p):AM1) method in combination with 52T and 64T cluster models for H-ZSM-5 and H-FER zeolites, respectively. All the results can be concluded as follows:

- (a) All the cracking mechanisms of *n*-pentane (C_5) and *n*-hexane (C_6) over the H-ZSM-5 and H-FER catalysts consist of two reaction pathways, namely the turnover and poisoning paths.
- (b) In all cases, the turnover path is kinetically much more preferred than the poisoning path.
- (c) The main products for the C_5 and C_6 cracking either on the H-ZSM-5 or H-FER zeolite are the 1,2-pentene (C_5^-) and 1,2-hexene (C_6^-), respectively. These results are in good agreements with experiments.
- (d) The reaction rates of zeolites for productions of C_5^- and C_6^- olefins at 298.15 K are in order: FER for C_5^- > FER for C_6^- > ZSM-5 for C_6^- > ZSM-5 for C_5^- . Thus, H-FER catalyst is more effective than H-ZSM-5 catalyst.

- [1] Komatsu, T., Ishihara, H., Fukui, Y., and Yashima, T. Selective formation of alkenes through the cracking of *n*-heptane on Ca²⁺-exchanged ferrierite. Applied Catalysis A: General 214(1) (2001): 103-109.
- [2] Degnan, T.F., Chitnis, G.K., and Schipper, P.H. History of ZSM-5 fluid catalytic cracking additive development at Mobil. Microporous and Mesoporous Materials 35–36 (2000): 245-252.
- [3] Rownaghi, A.A., Rezaei, F., and Hedlund, J. Selective formation of light olefin by *n*-hexane cracking over H-ZSM-5: Influence of crystal size and acid sites of nano- and micrometer-sized crystals. Chemical Engineering Journal 191 (2012): 528-533.
- [4] Miyaji, A., et al. Selective production of ethylene and propylene via monomolecular cracking of pentene over proton-exchanged zeolites: Pentene cracking mechanism determined by spatial volume of zeolite cavity. Journal of Catalysis 302 (2013): 101-114.
- [5] Lin, L., et al. Acid strength controlled reaction pathways for the catalytic cracking of 1-butene to propene over ZSM-5. Journal of Catalysis 309 (2014): 136-145.
- [6] Sun, Y.-X., Yang, J., Zhao, L.-F., Dai, J.-X., and Sun, H. A two-layer ONIOM Study on initial reactions of catalytic cracking of 1-butene to produce propene and ethene over H-ZSM-5 and H-FAU zeolites. Journal of Physical Chemistry 114(13) (2010): 5975-5984.
- [7] Guo, Y.-H., Pu, M., Chen, B.-H., and Cao, F. Theoretical study on the cracking reaction catalyzed by a solid acid with zeolitic structure: The catalytic cracking of 1-hexene on the surface of H-ZSM-5. Applied Catalysis A: General 455 (2013): 65-70.
- [8] Cormaa, A., Mengualb, J., and Miguelc, P.J. IM-5 zeolite for steam catalytic cracking of naphtha to produce propene and ethene. An alternative to ZSM-5 zeolite. Applied Catalysis A: General 460–461 (2013): 106-115.
- [9] Corma, A., Mengual, J., and Miguel, P.J. Stabilization of ZSM-5 zeolite catalysts for steam catalytic cracking of naphtha for production of propene and ethene. Applied Catalysis A: General 421–422 (2012): 121-134.

- [10] Luo, J., Bhaskar, B.V., Yeh, Y.-H., and Gorte, R.J. *n*-hexane cracking at high pressures on H-ZSM-5, H-BEA, H-MOR, and USY for endothermic reforming. Applied Catalysis A: General 478 (2014): 228-233.
- [11] Bastiani, R., Lam, Y.L., Henriques, C.A., and Silva, V.T.d. Application of ferrierite zeolite in high-olefin catalytic cracking. Fuel 107 (2013): 680-687.
- [12] Kissin, Y.V. Chemical mechanisms of catalytic cracking over solid acidic catalysts: Alkanes and alkenes. Catalysis Reviews: Science and Engineering 43(1-2) (2001): 85-146.
- [13] Swisher, J.A., Hansen, N., Maesen, T., Keil, F.J., Smit, B., and Bell, A.T. Theoretical simulation of *n*-alkane cracking on zeolite. Journal of Physical Chemistry C 114(22) (2010): 10229-10239.
- [14] Tranca, D.C., Hansen, N., Swisher, J.A., Smit, B., and Keil, F.J. Combined density functional theory and monte carlo analysis of monomolecular cracking of light alkanes over H-ZSM-5. Journal of Physical Chemistry C 116(44) (2012): 23408-23417.
- [15] Konno, H., Okamura, T., Kawahara, T., Nakasaka, Y., Tago, T., and Masuda, T. Kinetics of *n*-hexane cracking over ZSM-5 zeolites - effect of crystal size on effectiveness factor and catalyst lifetime. Chemical Engineering Journal 207-208 (2012): 490-496.
- [16] Urataa, K., Furukawab, S., and Komatsua, T. Location of coke on H-ZSM-5 zeolite formed in the cracking of *n*-hexane. Applied Catalysis A: General 475 (2014): 335-340.
- [17] Konno, H., Tago, T., Nakasaka, Y., Ohnaka, R., Nishimura, J.-i., and Masuda, T. Effectiveness of nano-scale ZSM-5 zeolite and its deactivation mechanism on catalytic cracking of representative hydrocarbons of naphtha. Microporous and Mesoporous Materials 175 (2013): 25-33.
- [18] Kubo, K., Iida, H., Namba, S., and Igarashi, A. Effect of steaming on acidity and catalytic performance of H-ZSM-5 and P/H-ZSM-5 as naphtha to olefin catalysts. Microporous and Mesoporous Materials 188 (2014): 23-29.
- [19] Xu, R., Pang, W., Yu, J., Huo, Q., and Chen, J. Chemistry of zeolites and related porous materials: Synthesis and structure. John Wiley & Sons (Asia) Pte Ltd, 2007.

- [20] Eder, F., Stockenhuber, M., and Lercher, J.A. Brønsted acid site and pore controlled siting of alkane sorption in acidic molecular sieves. Journal of Physical Chemistry B 101(27) (1997): 5414-5419.
- [21] Garcí'a-Pe' rez, E., Dubbeldam, D., Maesen, T.L.M., and Calero, S. Influence of cation Na/Ca ratio on adsorption in LTA 5A: A systematic molecular simulation study of alkane chain length. Journal of Physical Chemistry B 110 (2006): 23968-23976.
- [22] Van Bokhoven, J.A. Strong brønsted acidity in alumina-silicates. Influence of pore dimension, steaming and acid site density on cracking of alkanes. Ordered Porous Solids (2009): 657-668.
- [23] Akhmedov, V. and Al-Khowaiter, S. Recent advances and future aspects in the selective isomerization of high *n*-alkanes. Catalysis Reviews - Science and Engineering 49(1) (2007): 33-139.
- [24] Baerlocher, C., McCusker, L.B., and Olson, D.H. Zeolite framework types [Online]. Available from: www.iza-structure.org/databases [20 November 2015].
- [25] Well, W.J.M.v., et al. Chain length effects of linear alkanes in zeolite ferrierite. 1. Sorption and ¹³C NMR experiments. Journal of Physical Chemistry B 102(20) (1998): 3945-3951.
- [26] Levine, I.N. Quantum chemistry. 5th ed.: Prentice-Hall, Inc, 2000.
- [27] Atkins, P. and Friedman, R. Molecular quantum mechanics. Oxford University Press Inc., 2005.
- [28] Lewars, E. Computational chemistry : Introduction to the theory and applications of molecular and quantum mechanics. Kluwer Academic, 2003.
- [29] Dappricha, S., Komáromia, I., Byuna, K.S., Morokumaa, K., and Frischb, M.J. A new ONIOM implementation in Gaussian98. Part I. The calculation of energies, gradients, vibrational frequencies and electric field derivatives. Journal of Molecular Structure (Theochem) 461-462 (1999): 1-21.
- [30] Levine, R.D. Molecular reaction dynamics. Cambridge University Press, 2005.
- [31] Ochterski, J.W. Thermochemistry in Gaussian. Gaussian Inc. (2000).
- [32] Bravo-Perez, G., Alvarez-Idaboy, J.R., Cruz-Torres, A., and Ruiz, M.E. Quantum chemical and conventional transition-state theory calculations of

- rate constants for the NO^{3+} alkane reaction. Physical Chemistry A106 (2002): 4645-4650.
- [33] Ruangpornvisuti, V. A DFT study of transformation of nitrosothiol isomers and their decomposition to nitric oxide in gas phase. International Journal of Quantum Chemistry 109 (2009): 275-284.
- [34] Wigner, E. Über das Überschreiten von potentialschwellen bei chemischen reaktionen. Journal of Physical Chemistry B19 (1932): 203-216.
- [35] Hirschfelder, J.O. and Wigner, E. Some quantum mechanical considerations in the theory of reactions involving an activation energy. Journal of Chemical Physics 7 (1939): 616-628.
- [36] Humbel, S., Sieber, S., and Morokuma, K. The IMOMO method: Integration of different levels of molecular orbital approximations for geometry optimization of large systems: Test for *n*-butane conformation and $\text{S}_{\text{N}}2$ reaction: $\text{RCl}+\text{Cl}^-$. Journal of Physical Chemistry 105 (1996): 1959–1967.
- [37] Maseras, F. and Morokuma, K. IMOMM: A new integrated ab initio+ molecular mechanics geometry optimization scheme of equilibrium structures and transition states. Journal of Computational Chemistry 16 (1995): 1170-1179.
- [38] Becke, A.D. Density-functional thermochemistry. III. The role of exact exchange. Journal of chemical Physics 98 (1993): 5648-5652.
- [39] Lee, C., Yang, W., and G.Parr, R. Development of the Colle-Salvetti correlation-energy formula into a function of the electron density. Physical Review B 37(2) (1988): 785-789.
- [40] McLean, A.D. and Chandler, G.S. Contracted Gaussian basis sets for molecular calculations. I. Second row atoms, $Z=11-18$. Journal of Chemical Physics 72 (1980): 5639-5648.
- [41] Dewar, M.J.S. and Reynolds, C.H. An improved set of mndo parameters for sulfur. Journal of Computational Chemistry 2 (1986): 140-143.
- [42] Frisch, M.J., et al. Gaussian 09, Revision D.01. 2014, Gaussian Inc., Wallingford, CT.
- [43] Flükiger, P., Lüthi, H.P., Portmann, S., and Weber, J. MOLEKEL 4.3. 2000: Swiss Center for Scientific Computing, Manno, Switzerland.

- [44] Koningsveld, H.V., Bekkum, H.V., and Jansen, J.C. On the location and disorder of the tetrapropylammonium (TPA) ion in zeolite ZSM-5 with improved framework accuracy. Acta Crystallographica B43 (1987): 127-132.
- [45] Baerlocher, C., McCusker, L.B., and Olson, D.H. Atlas of zeolite framework types. Sixth revised ed.: Elsevier Science, 2007.
- [46] Pu, S.B. and Inui, T. Diffuse reflectance i.r. spectroscopic study on hydroxyl groups of H-ZSM-5s having different sizes and properties. Zeolites 19 (1997): 452-454.



REFERENCES





APPENDICES

จุฬาลงกรณ์มหาวิทยาลัย
CHULALONGKORN UNIVERSITY

Table A-1 Optimized geometrical distances (in Å) between atoms of H-ZSM-5 and interacting species for reaction path of *n*-pentane (C₅) conversion to 1,2-pentene (C₅[≡]) over the H-ZSM-5 catalyst.

	C1 ^a -C2 ^a	C2 ^a -C3 ^a	C1 ^a -H3 ^a	C2 ^a -H2 ^a	C2 ^a -H1 ^b	O1 ^b -H1 ^b	O3 ^b -H3 ^a	H1 ^b -H2 ^a
C ₅ /HZ ^Z	1.533	1.535	1.094	1.101	2.382	0.971	4.807	1.914
TS1_ _Z ^Z	1.520	1.525	1.091	1.153	2.071	1.718	4.219	0.952
C ₅ ⁺ /Z ^{Z-}	1.434	1.491	1.129	-	-	-	1.938	0.850
TS2_ _Z ^Z	1.420	1.500	1.266	-	-	-	1.493	0.743
C ₅ [≡] /Z ^Z H	1.340	1.503	2.523	-	-	-	0.989	0.743

^a interacting species for reaction path of *n*-pentane (C₅) conversion to 1,2-pentene (C₅[≡]).

^b atoms of H-ZSM-5 catalyst.

Table A-2 Optimized geometrical distances (in Å) between atoms of H-ZSM-5 and interacting species for reaction path of *n*-hexane (C₆) conversion to 1,2-hexene (C₆[≡]) over the H-ZSM-5 catalyst.

	C1 ^a -C2 ^a	C2 ^a -C3 ^a	C1 ^a -H3 ^a	C2 ^a -H2 ^a	C2 ^a -H1 ^b	O3 ^b -H3 ^a	O1 ^b -H1 ^b	H1 ^b -H2 ^a
C ₆ /HZ ^Z	1.534	1.534	1.095	1.101	2.374	4.811	0.977	1.915
TS1' _Z ^Z	1.528	1.541	1.092	1.269	1.392	4.120	1.714	0.962
C ₆ ⁺ /Z ^{Z-}	1.420	1.459	1.154	-	-	1.849	-	0.844
TS2' _Z ^Z	1.387	1.474	1.273	-	-	1.486	-	0.743
C ₆ [≡] /Z ^Z H	1.341	1.501	2.430	-	-	0.990	-	0.743

^a interacting species for reaction path of *n*-hexane (C₆) conversion to 1,2-hexene (C₆[≡]).

^b atoms of H-ZSM-5 catalyst.

Table A-3 Optimized geometrical distances (in Å) between atoms of H-FER and interacting species for reaction path of *n*-pentane (C₅) conversion to 1,2-pentene (C₅[≡]) over the H-FER catalyst.

	C1 ^a -C2 ^a	C2 ^a -C3 ^a	C1 ^a -H3 ^a	C2 ^a -H2 ^a	C2 ^a -H1 ^b	O1 ^b -H1 ^b	O5 ^b -H3 ^a	H1 ^b -H2 ^a
C ₅ /HZ ^F	1.532	1.536	1.096	1.101	2.156	0.984	4.583	1.807
TS1_Z ^F	1.537	1.538	1.094	1.216	1.373	1.406	3.794	1.089
C ₅ ⁺ /Z ^{F,-}	1.437	1.452	1.125	-	-	-	2.009	0.860
TS2_Z ^F	1.383	1.476	1.307	-	-	-	1.398	0.743
C ₅ [≡] /Z ^F H	1.342	1.502	2.271	-	-	-	0.997	0.743

^a interacting species for reaction path of *n*-pentane (C₅) conversion to 1,2-pentene (C₅[≡]).

^b atoms of H-FER catalyst.

Table A-4 Optimized geometrical distances (in Å) between atoms of H-FER and interacting species for reaction path of *n*-hexane (C₆) conversion to 1,2-hexene (C₆[≡]) over the H-FER catalyst.

	C1 ^a -C2 ^a	C2 ^a -C3 ^a	C1 ^a -H3 ^a	C2 ^a -H2 ^a	C2 ^a -H1 ^b	O1 ^b -H1 ^b	O5 ^b -H3 ^a	H1 ^b -H2 ^a
C ₆ /HZ ^F	1.535	1.534	1.095	1.099	2.227	0.981	4.583	1.914
TS1'_Z ^F	1.539	1.539	1.094	1.195	1.313	1.777	3.794	0.977
C ₆ ⁺ /Z ^{F,-}	1.442	1.446	1.120	-	-	-	2.085	0.850
TS2'_Z ^F	1.383	1.476	1.319	-	-	-	1.389	0.743
C ₆ [≡] /Z ^F H	1.343	1.501	2.048	-	-	-	1.000	0.743

^a interacting species for reaction path of *n*-hexane (C₆) conversion to 1,2-hexene (C₆[≡]).

^b atoms of H-FER catalyst.

Table A-5 Partition functions, Tunneling coefficients (κ) and A factors in the *n*-pentane cracking over the H-ZSM-5 catalyst.

Conversion reaction	Q_{TS}/Q_{REA}	κ	A
Adsorption			
$C_5+HZ^Z \rightarrow C_5/HZ^Z$	-	-	-
Progressive conversion			
$C_5/HZ^Z \rightarrow TS1_Z^Z \rightarrow C_5^+/Z^{Z-} + H_2$	3.82×10^{-2}	2.48	2.39×10^{11}
$C_5^+/Z^{Z-} \rightarrow TS2_Z^Z \rightarrow C_5^=/Z^ZH$	2.07×10^0	1.13	1.29×10^{13}
Alkoxy species formation			
$C_5^+/Z^{Z-} \rightarrow TS3_Z^Z \rightarrow C_5/Z^Z$	8.91×10^{-1}	1.00	5.53×10^{12}
Desorption			
$C_5^=/Z^ZH \rightarrow C_5^= + Z^ZH$	-	-	-

Table A-6 Partition functions, Tunneling coefficients (κ) and A factors in the *n*-hexane cracking over the H-ZSM-5 catalyst.

Conversion reaction	Q_{TS}/Q_{REA}	κ	A
Adsorption			
$C_6+HZ^Z \rightarrow C_6/HZ^Z$	-	-	-
Progressive conversion			
$C_6/HZ^Z \rightarrow TS1_Z^Z \rightarrow C_6^+/Z^{Z-} + H_2$	6.39×10^{-2}	1.55	3.97×10^{11}
$C_6^+/Z^{Z-} \rightarrow TS2_Z^Z \rightarrow C_6^=/Z^ZH$	2.40×10^{-1}	1.17	1.49×10^{12}
Alkoxy species formation			
$C_6^+/Z^{Z-} \rightarrow TS3'_Z^Z \rightarrow C_6/Z^Z$	1.18×10^{-1}	1.01	7.32×10^{11}
Desorption			
$C_6^=/Z^ZH \rightarrow C_6^= + Z^ZH$	-	-	-

Table A-7 Partition functions, Tunneling coefficients (κ) and A factors in the *n*-pentane cracking over the H-FER catalyst.

Conversion reaction	Q_{TS}/Q_{REA}	κ	A
Adsorption			
$C_5 + HZ^F \rightarrow C_5/HZ^F$	-	-	-
Progressive conversion			
$C_5/HZ^F \rightarrow TS1_Z^F \rightarrow C_5^+/Z^{F-} + H_2$	1.33×10^{-1}	2.04	8.28×10^{11}
$C_5^+/Z^{F-} \rightarrow TS2_Z^F \rightarrow C_5^=/Z^FH$	1.07×10^{-1}	1.58	6.64×10^{11}
Alkoxy species formation			
$C_5^+/Z^{F-} \rightarrow TS3_Z^F \rightarrow C_5/Z^F$	8.38×10^{-1}	1.01	5.20×10^{12}
Desorption			
$C_5^=/Z^FH \rightarrow C_5^= + Z^FH$	-	-	-

Table A-8 Partition functions, Tunneling coefficients (κ) and A factors in the *n*-pentane cracking over the H-FER catalyst.

Conversion reaction	Q_{TS}/Q_{REA}	κ	A
Adsorption			
$C_6 + HZ^F \rightarrow C_6/HZ^F$	-	-	-
Progressive conversion			
$C_6/HZ^F \rightarrow TS1_Z^F \rightarrow C_6^+/Z^{F-} + H_2$	1.17×10^{-1}	1.38	7.26×10^{11}
$C_6^+/Z^{F-} + H_2 \rightarrow TS2_Z^F \rightarrow C_6^=/Z^FH + H_2$	3.11×10^{-1}	1.70	1.93×10^{12}
Alkoxy species formation			
$C_6^+/Z^{F-} \rightarrow TS3'_Z^F \rightarrow C_6/Z^F$	2.11×10^{-2}	1.02	1.31×10^{11}
Desorption			
$C_6^=/Z^FH + H_2 \rightarrow C_6^= + Z^FH + H_2$	-	-	-

VITA

Name Miss PRAPAPORN KITTIWATTANASAK

Date of Birth October 7th, 1989

Place of Birth Phitsanulok, Thailand

Address 21/5 Moo 2, Tambon Tatong, Amphoe Mueang,
Phitsanulok 65000

Telephone 089-8598679

E-mail address prapaporn.kit@gmail.com

Educations

2012-2016 M.Sc. (Petrochemistry and Polymer science),
Chulalongkorn University, Thailand

2008-2012 B.Eng. (Petrochemical and Polymeric material),
Silapakorn University, Thailand

2002-2008 Janokrong high school, Phitsanulok, Thailand

1994-2002 Rojanawit Malabiang school, Phitsanulok, Thailand

Proceeding

Catalytic cracking of n-hexane to olefins using H-ZSM-5
and H-FER (Poster Session): PETROMAT and
PPC SYM 2015, Tuesday April 21, 2015,
Chamchuri 10 Building Chulalongkorn University
Bangkok, Thailand.



จุฬาลงกรณ์มหาวิทยาลัย
CHULALONGKORN UNIVERSITY